minerals

IMPACT FACTOR 2.5

CITESCORE 3.9

Article

3D Modelling Approach to Enhance the Characterization of a Bronze Age Nuragic Site

Stefano Cara, Paolo Valera and Carlo Matzuzzi

Special Issue

Multidisciplinary Research for the Monitoring and Preventive Conservation of Cultural Heritage

Edited by

Dr. Silvana Fais and Dr. Giuseppe Casula

MDPI

https://doi.org/10.3390/min14050489

minerals

MDPI

Article

3D Modelling Approach to Enhance the Characterization of a Bronze Age Nuragic Site

Stefano Cara [1], Paolo Valera [2] and Carlo Matzuzzi [1,*]

[1] National Research Council of Italy—Institute of Environmental Geology and Geoengineering (IGAG), 09124 Cagliari, Italy; stefano.cara@cnr.it
[2] Department of Civil and Environmental Engineering and Architecture (DICAAR), University of Cagliari, 09124 Cagliari, Italy; pvalera@unica.it
* Correspondence: carlo.matzuzzi@igag.cnr.it

Abstract: Megalithism in Sardinia (Italy) had its highest expression during the Bronze Age with the creation of monumental complexes known as Nuraghes. These unique monuments have recently been the subject of in-depth investigations for their potential to be recognized as World Heritage Sites (by UNESCO). The main purpose of our research was to make a contribution to obtain a more in-depth characterization of these monuments by testing a 3D model of a complex Nuraghe, integrated with an analysis of the geolithological context. This work first focused on the geological and typological investigation of the materials used in its construction, which was then compared with the geolithological characteristics of the region. A survey of the outcropping remains was carried out by means of Structure-from-Motion Multi-View Stereo (SfM-MVS) photogrammetry with UAV ground and aerial acquisition using APS-C photo sensors, georeferenced with an RTK-GNSS ground survey. The level of accuracy of our digital models shows the potential of the proposed method, giving accurate and geometrically consistent 3D reconstructions in terms of georeferencing error, shape and surface. The survey method allows for the virtualization of the current state of conservation of the Nuraghe, giving a solid basis to set up further (future) archaeological excavations and to contribute to knowledge on the architecture of the structures. This study also provides useful information on the nature and origin of the construction materials and proposes a hypothesis on the original dimensions of the monument, which is often a topic of debate in the world of archaeology.

Keywords: UAV; RPAS; photogrammetry; geoarchaeology; 3D reconstruction; virtual archaeology; Nuraghe

Citation: Cara, S.; Valera, P.; Matzuzzi, C. 3D Modelling Approach to Enhance the Characterization of a Bronze Age Nuragic Site. *Minerals* **2024**, *14*, 489. https://doi.org/10.3390/min14050489

Academic Editor: Adrián Durán Benito

Received: 1 April 2024
Revised: 30 April 2024
Accepted: 30 April 2024
Published: 6 May 2024

1. Introduction

The purpose of this work was to obtain a more in-depth characterization of Nuraghes, the unique and identifying monuments of the Nuragic civilization developed during the Bronze Age in Sardinia (Italy). These monuments are currently the subject of in-depth scientific studies for the purpose of their recognition as UNESCO World Heritage Sites. This study's results allowed for the development of an experimental survey method based on UAV platform-based photogrammetric survey and 3D modelling techniques applied to a complex Nuraghe. This study was integrated with an analysis of the geolithological context to provide useful information on the nature and origin of the building materials and to propose a realistic hypothesis on the original proportions and dimensions of the monument, based on the morphometric analysis of the virtual models obtained. The Nuragic civilization developed in Sardinia mainly during the Bronze Age (18th–10th century BC). The naming of this civilization does not refer directly to an ethnic subject nor to a major ideal current but rather to the impressive and unique architectural phenomenon of megalithic towers, known in the local language as "Nuraghes" [1–4].

The Nuraghes, with about 8000 currently characterized in Sardinia, have undergone a remarkable architectural evolution, starting from the earliest and simplest form of so-called

"archaic Nuraghes". It is precisely from the evolution of these archaic Nuraghes—in a phase of the Middle Bronze Age about which scholars still debate, between the 17th and 14th centuries BC—that led to the definition of the tower-shaped nuraghe form, with a large central chamber [5]. This first phase of evolution was followed by a second one (late 14th–11th century BC), in which the building knowledge of the Nuragic people became intertwined with the experiences of Aegean architects, since circular chambers, corridors, and large ogival vaults are common to Sardinia, the island of Crete, and mainland Greece [6,7]. Nuraghes can be mainly represented by three types: the so-called archaic Nuraghes, developed from the beginning on one level with corridors and chambers without a vaulted enclosure; the single-tower Nuraghe, containing one or more vaulted chambers; and the more evolved construction of the complex polylobate Nuraghe [5]. Thus, the basic construction concept of the most evolved Nuraghe is centered on the construction of the truncated conical tower with a chamber, made using the technique of drystone masonry by laying concentric rows of polygonal stone boulders, slightly projecting towards the center, until obtaining the vaulted closure of the chamber, called "a tholos". The use of the term "tholos" in our paper refers to the construction characteristic of the architectural structure. This term is used extensively in archaeology, and particularly by scholars of Sardinian archaeology, in reference to the construction of Nuragic tower chambers to refer to a circular, truncated-cone-shaped construction consisting of rings of projecting stone blocks forming a pseudo-dome [8]. The megalithic structure of the wall usually consists of blocks with decreasing size from the bottom to the top: the larger ones are arranged according to a so-called "cyclopean" polygonal structure and are arranged in more or less regular overlapping rows to form the base, while for the upper part of the masonry, elements in many cases are placed in an "isodomic" arrangement, so as to obtain a better distribution of loads and more easily allow for the curved profile of the vault [5]. For the construction of Nuraghes, local stone materials were usually used. The nature and characteristics of these materials certainly influenced the aesthetic appearance and durability of the constructions, but they certainly did not prevent ancient builders from constructing their monuments even with materials that were difficult to work with, while maintaining the basic architectural and structural characteristics. The construction of the walls is in itself very complex and involved not only the laying of boulders of considerable size but also the use of stones mixed with earth of various nature and granulometry, intended to fill in the voids, to make the wall structure more homogeneous and stable and insulate it from the outside. The outer walls of the towers show a varied inclination (usually less than 10°), which in some cases is not constant but decreases strongly in the upper part of the structure (as found in the Nuraghe Nuraddeo of Suni [5]). The module of the inner tholos chamber was generally replicated upward with the same proportions, but with reduced dimensions, and could also develop on three superimposed levels (such as the Nuraghe Santu Antine in Torralba) giving rise to towers of considerable height. However, to date, in no Nuraghe has the summit part (probably consisting of a terrace) been found intact; therefore, it is not possible to define exactly the maximum height originally reached by the Nuragic towers. Hypotheses about the characteristics of the summit structure have been made by past studies based on stylized Nuraghe artefacts (bronze and lithic) that show the presence above the towers of a terrace with a balcony projecting from the masonry and supported by brackets, found, for example, in large numbers in the archaeological area of "Su Nuraxi" in Barumini [1,9].

The typical structure of the Nuragic tower includes at least three basic characterizing elements: the access door lintel, the access corridor, and the so called "a tholos" chamber. The other distinctive element is the staircase, usually with helicoidal development and built within the masonry of the tower itself, allowing access to the upper level(s). However, stairs have not been found in all Nuraghes, either because of their state of ruin or because it is effectively absent [5]. In more advanced Nuragic structures, a turreted walled enclosure (a sort of bulwark) was added and developed harmoniously around the main monument. Complex Nuraghes reached their greatest number and highest magnificence and elegance

in the period between the Recent and Final Bronze Ages (about 1350 and 1100 BC); among them, about 40–50 are shown to be surrounded entirely by a wall with towers that are only one floor high. Therefore, the outer towers were under the control of the rampart and its main tower, which reached greater heights [6]. Nuraghes are found to be widespread throughout the Sardinian territory, from the coasts to the Gennargentu massif (central Sardinia), but they are more frequently found in the interior areas of the island. On the other hand, they tend to be less frequent in the areas in the middle of the Campidano plain (south-central Sardinia) and in the today's wooded reliefs [6]. In the present work, we studied a complex Nuraghe located in the territory of south Sardinia (Sa Domu e S'Orku in Domusnovas). This Nuraghe was already characterized in the second half of the 1800s [10,11] and described in more detail in subsequent work presented in the 1960s and 1980s [1]. This monument consists of a main tower with a bastion with polylobate development and a front courtyard. The main structure is included within a discontinuous wall with five perimeter towers (Figure 1). The masonry work is of the polyhedral type, with stone blocks arranged tendentially in oblique rows, forming a so-called "megalithic matrix" [1]. The masonry structures of the Nuragic complex consist of a double stone face of irregular (unworked or slightly hewed) blocks that show dimensional variability ranging from just under a meter to two meters and decreasing from the bottom to the top. The interior space of the masonry is occupied by rubble stone mixed with loose material of varying grain size. The internal tholos chambers of the towers have access corridors, niches, and, in the case of the main tower, a spiral staircase (currently not accessible because it is occluded by collapses) that led to the upper level [1].

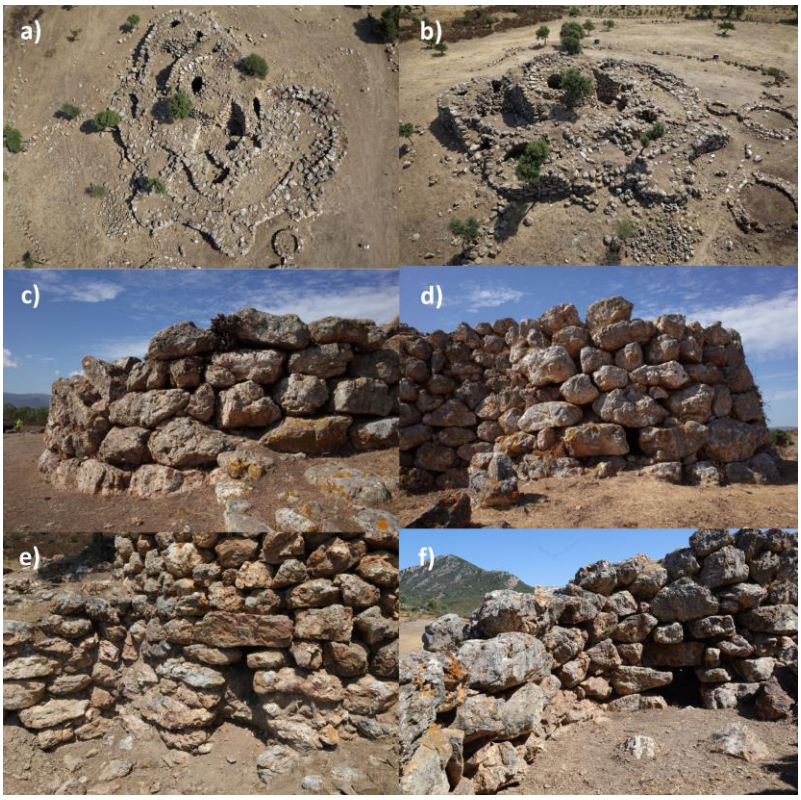

Figure 1. The archaeological site of Nuraghe Sa Domu e S'Orku, Domusnovas. The images highlight the texture and complexity of the monument's forms and surfaces. (**a**,**b**) aerial views; (**c**) view from the south; (**d**) view from the north; (**e**) main tower entrance; (**f**) west court and northern tower.

In this work, we have implemented and tested 3D modelling integrated with the geolithological investigation of the area to improve the characterization of the Nuragic site. This study focused particularly on the geometric and dimensional characterization

of the Nuragic structures still in place and on the typological definition of the materials used for their construction, within the geolithological context of the photogrammetric survey area and its surroundings. The effectiveness of this integrated approach has already been highlighted at the scale of the archaeological artifact. Some authors report schematic references of the architectural proportions of Nuraghes, reporting the main measured quantities and significant dimensional parameters used to describe and compare structures and to understand the variety of Nuragic architecture in relation to building types and techniques [10]. Dimensional analyses of these monuments are often presented in descriptive and qualitative terms, without a systematic study of the relationships and proportions between architectural elements [12]. In the present study, the geometric parameters of the Nuraghe were surveyed and measured in a systematic way, highlighting, in particular, the importance of carrying out an analysis of the unevenness of the terrain, which should also be reported below the architectural structure (obtained by correlating the RTK-GNSS topographic survey data with those obtained from the 3D photogrammetric models). This is in order to obtain the definition of the original elevation of the accesses to the towers and the walled enclosure by estimating the thicknesses of the collapses within the structures. These survey methods are also used to carry out the measurements and analysis of the proportions of the collapsed or partially buried parts as well.

3D modelling based on Structure-from-Motion Multi-View Stereo (SfM-MVS) techniques particularly in recent years has had a significant uptake in the field of digital documentation and the mapping of cultural heritage sites [13–16]. Numerous studies have shown that SfM-MVS photogrammetry, by optimizing the acquisition phase, can achieve levels of accuracy and completeness of 3D models comparable to those achievable through scanning (LiDAR) and laser scanning (TLS), presenting several advantages in terms of cost, the speed of data acquisition, processing, and the quality of both geometric and photorealistic 3D models [14,17]. Photogrammetry allows for operational flexibility with acquisition from multiple viewpoints by limiting the shadow areas and blind spots generated by occlusions, which are typical of laser scanner surveys. Topographic mapping at different scales is usually based on the use of a laser total station (TS), global navigation satellite system (GNSS), terrestrial laser scanning (TLS), and LiDAR scanning [18]. In areas with special morphological complexities, mapping is increasingly being performed using UAV systems equipped with full-frame DSLR and APS-C photographic sensors using SfM-MVS photogrammetric techniques. Using different approaches to SfM-MVS modeling, it is possible to reconstruct 3D models of an object based on the extraction of data obtained from sequences of 2D photographs taken with overlapping acquisitions, even using photos captured with uncalibrated cameras by varying the point of view angle [17–19]. In areas with particular morphological complexities and brightness problems, mapping is performed by nadiral and oblique image acquisition using UAV equipped with full-frame or APS-C cameras [17,18,20–22]. Large-scale systematic deformation can be reduced with the use of a network of ground control points (GCPs) [23]. Several authors have analyzed the influence of image overlap and the number and distribution of GCPs used for georeferencing 3D models as key aspects with respect to the accuracy of 3D reconstruction. In addressing the issues of the 3D modelling of cultural heritage sites, several authors have highlighted the advantages of SfM-MVS modeling also integrated with diagnostic material analysis techniques [15,18,23–25]. Photogrammetric surveys based on the use of UAV platforms are documented in the literature for the creation of digital models that, thanks to the use of various photogrammetric software available on the market, allow the generation of 3D models, DTM and DSM models, ortho-photos, and high-resolution topographic maps of artefacts and structures in archaeological and cultural heritage fields (but also for topographic mapping, monitoring, and the analysis of the degradation of monuments and structures for geomorphological analysis) [18,23,26–28]. At present, 3D recordings of prehistoric archaeological monuments in Sardinia (Italy) have only been carried out for a few cases. Among them, it is important to mention the Nuraghe Oes project [29], which provided a complete documentation of the state of conservation of a complex Nuraghe,

adding to the archaeological knowledge about the nature of the monument, using several integrated geomatic techniques [29]. The precision of 3D SfM-MVS models processed from digital photogrammetric images depends on several factors such as the quality characteristics of the sensor, the lens focal length, the flight planning parameters of the UAV, the repeatability of the acquisition patterns, the orientation of the camera, the final quality of the images, the topographical and morphological characteristics of the area to be surveyed, the light conditions, the type and quality of the photogrammetric processing software used, as well as the distribution and quantity of ground control points and check points (GCPs and CPs) [27]. For applications requiring a greater precision of structures and architectural elements representation, the processing of the SfM-MVS 3D model can be implemented through an additional photogrammetric survey with a lower GSD (cm/pixel) integrated with LiDAR scanning and terrestrial TLS acquisitions to achieve greater levels of completeness and detail of 3D models especially in particularly complex structures [13,30]. The 3D models produced with these processing techniques enable the noninvasive metrological analysis of structures correlated with building materials' characterization, which can be applied in archaeology, conservation, and architecture fields. Such models can be used as basic tools for the planning of restoration work, maintenance scheduling, and documentation during archaeological excavations. They also allow for the creation of virtual reconstructions of partially collapsed or buried structures, providing useful insights for scholars about their original appearance. In addition, 3D reconstructions are effective for developing virtual and augmented reality (VR/AR) experiences, becoming additional tools for the enhancement and enjoyment of archaeological heritage even remotely through social media. Modelling techniques based on 3D SfM-MVS reconstruction can provide levels of accuracy comparable to those achievable with LiDAR scanning and laser scanner (TLS) acquisition, also providing an important contribution to digital documentation for the preservation of cultural heritage projects. These laser surveying techniques can be complementary to photogrammetric processing for the analysis and understanding of monuments, meeting versatility and accuracy requirements that allow for their integration into archaeological heritage enhancement studies [17,30].

2. Materials and Methods

2.1. Archaeological Site and Geographical Location

The archaeological site of the Nuraghe Sa Domu e S'Orku is located in the territory of the Municipality of Domusnovas (SU) and has a total extension of 26,000 m^2 (Figure 2). The photogrammetric survey area is geographically identified by the following vertices: 4,352,960.45 N, 1,468,931.67 E and 4,352,670.45 N, 1,469,121.67 E (Monte Mario/Italy Zone 1, EPSG:3003), corresponding to a total of about 0.0551 km^2 with a maximum elevation difference of about 17 m ($155 \leq Z \leq 138$ m). In this area, we can find the main monument that covers a total area of 1591 m^2, consisting of the Nuraghe with a bastion and central main tower (called the keep) surrounded by a wall equipped with five perimeter towers. Around the Nuraghe, there are several huts' remains, piles of stone blocks, and masonry remains, with a total area of about 6400 m^2. At the site, we distinguished a monument survey area with an extent of 80 × 80 m and a topographic mapping area extended to the entire archaeological site of 190 × 290 m. The dense vegetation cover, present at the time of the study, was removed as far as possible from the monument but remained scattered throughout the rest of the archaeological area. For the photogrammetric survey, the monument was divided into exterior and interior scenes. The size of the exterior scene was about 80 × 80 m and developed with a difference in elevation of about 15 m ($155 \leq Z \leq 140$ m). The interior scene includes accessible tholos chambers, their entrances, and corridors, where the maximum capture distance was less than 5 m.

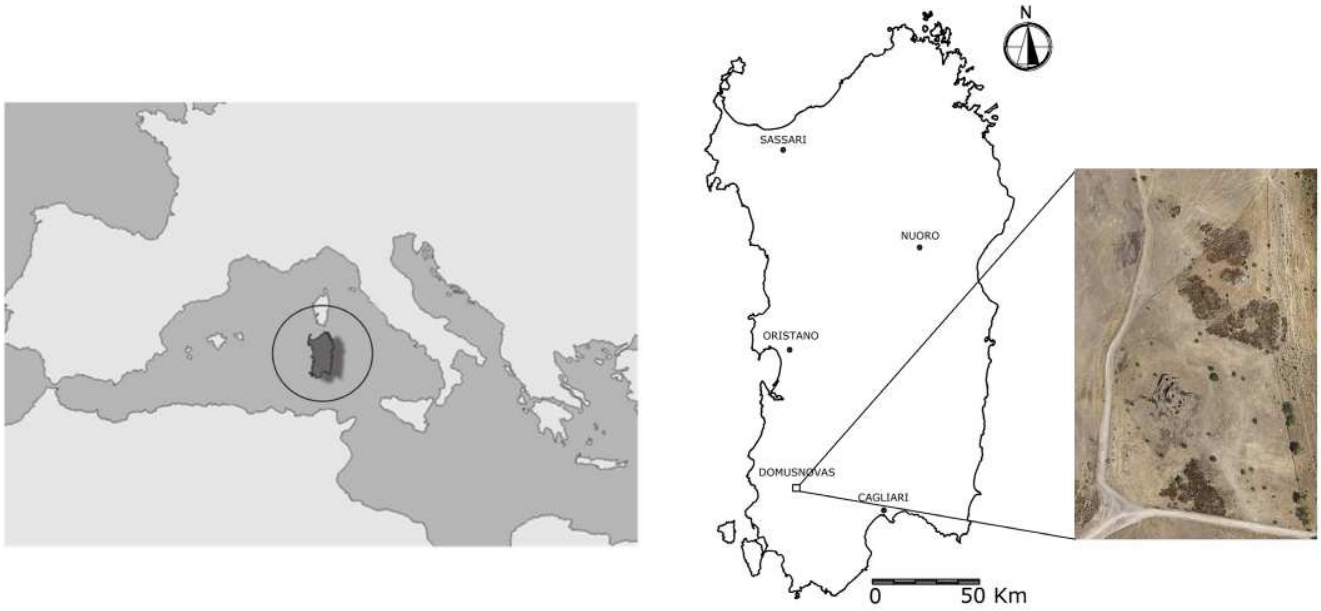

Figure 2. Geographical location of the archaeological site Sa Domu e S'Orku, Domusnovas.

2.2. Survey and Modelling Workflow

The adopted 3D surveying and modelling method was based on a workflow that involved defining the level of accuracy and visual quality required by the final 3D model. This depended on the minimum detail of the architectural elements of interest to be reproduced and the scale of the monument. The photogrammetric survey was performed with a UAV equipped with an APS-C sensor and developed following both nadiral parallel photogrammetric patterns and oblique converging shots. The UAV survey was integrated with ground details for partially covered and interior areas, following a scheme for parallel image sequences, which was acquired with normal and oblique axes to ensure the best base-to-height (B/H) ratio in the different capture situations [20,28]. The reconstruction of the 3D SfM-MVS model was carried out with reality capture software (RC) Version 1.3.1.117316 [31], subsequently simplified into sub-regions for visual and dimensional analysis at different scales. The quality validation of the 3D model is a key aspect. The estimation of errors in the georeferencing of shapes in terms of the 3D model's rigidity are verified by measurements on GCPs and CPs materialized using coded targets and measured using RTK-GNSS [17,30,32–34]. Surface accuracy can be estimated through comparison with benchmarks from the laser scanner survey (TLS) or the repeatability of the SfM-MVS process with the same APS-C sensor or full-frame sensor, along with the evaluation of completeness and the visual quality of textures [27,28,35].

The 3D SfM-MVS model obtained using the proposed workflow can achieve a level of accuracy consistent with the purposes of geometric and dimensional documentation and analysis at the scale of the archaeological monument. In addition to the 3D models, DTM and DSM, ortho-photos, and topographic maps, ortho-views are processed on characteristic sections and profiles of the monument so that measurements and comparisons can be made at the local scale. The methodology used for surveying and processing the 3D SfM-MVS model can be repeated systematically for other structures for typological and dimensional comparison.

2.3. UAV Survey and Photogrammetric Method

UAV flight planning for the aero-photogrammetric survey was carried out using Mikrokopter-Tool software, version 2.22 [36]. The survey was carried out according to flight plans with nadiral parallel shots and converging shots following circular orbits in accordance with the established optimal GSD, taking into account the variation in terrain and monument elevation. The value of the GSD for the oblique converging images was defined according to the average calculated over the overall values obtained, which considers the ground footprints of the camera image taken at the minimum and maximum distance from the object [20]. In-flight images were acquired with a Mikrokopter quadcopter [36], equipped with a Ricoh GR II camera (Table 1).

Table 1. UAV system and camera specifications.

UAV Parameters	Value	Camera Parameters	Value
Type	ARF-Mikrokopter	Sensor type	APS-C
Rotors	Quadro	Resolution (Mpix)	16.1
Size W × L × H (cm)	75 × 75 × 40	Focal length (mm)	18.3
Voltage (V)	14.8	Focal length equivalent (mm)	29.0
Battery (Mha)	LiPO 7200	Length sensor (mm)	15.6
MTOW (Kg)	2.8	Width sensor (mm)	23.7
Max flight time (min)	15	Pixel size (micron)	3.9
GPS navigation	U-BLOX MTK	Length frame (pix)	3264
Camera sensor	APS-C	Width frame (pix)	4928
Spectral range	RGB	Shot	Intervalometer

The nadiral flights over the archaeological area were oriented in the north–south direction and performed at altitudes of 30 m and 50 m, achieving coverage areas of 6400 m^2 and 55,100 m^2, respectively. The convergent shots were performed over the monument following circular flights orbits with the camera inclined at $15° \leq \alpha \leq 60°$ at different altitudes of $10 \leq Q \leq 45$ m. During flight in the real operational scenario, the camera altitude and pointing direction are always subject to some degree of variability from the theoretical planned flight lines (camera in nadiral or convergent orientation). This aspect generates a random noise component related to small variations in camera pointing direction (due to UAV roll, pitch, and yaw movements) or distance (altitude) variations related to terrain slope trends [23]. Converging image acquisition according to a circular orbit is shown in several studies to be particularly effective in reducing doming error [23]. Flight plans along parallel lines were programmed with an 85% overlap and 75% sidelap, set in accordance with the parameters of the camera used (sensor size, focal length, and flight altitude). At flight altitudes of 30 m and 50 m, B/H values were within the allowable range of <0.30. The same applied for the survey with circular orbits at altitudes in the range of $10 \leq Q \leq 35$ m with B/H values of <0.25. The camera was set in aperture priority mode, fixed to f/8 for nadir images and f/5.6 for oblique images and with a shutter speed of 1/1000 s. All images were captured in RAW format with ISO set to 250. To complement the UAV shots, images from the ground were also acquired with the same APS-C sensor. The use of parallel and oblique images is equally valid for ground-based image collection with consistent B/H ratio values and camera-to-object distance in the range of $1 \leq D \leq 5$ m [23,28]. When the survey targets indoor scenes and confined environments or transition zones between different scenes with illumination variability, image shooting becomes problematic in terms of acquisition mode and data quality. In such scenes, the field of view (FOV) of each photo turns out to be limited. This aspect affects the B/H ratios, whose correct setting is the basis for the photogrammetric accuracy expected with the overall specifications defined in the survey. The total number of images acquired in flight was 2128, while 1331 photos were taken from the ground, for a total of 3459. The average GSD in the survey area is 1.00 cm/pixel, and the average GSD in the monument area is 0.53 cm/pixel.

The total time to complete all acquisitions was 4 h, from UAV setup to the end of the survey. The RTK-GNSS surveys of GCPs and CPs control points, including ground points, were collected on geological outcrops. RAW images were post-processed to improve their quality by adjusting white balance, color correction, noise reduction, and exposure compensation parameters. Images acquired during the photogrammetric survey were processed using reality capture software [31] based on Structure-from-Motion Multi-View Stereo (SfM-MVS). 3D photogrammetric reconstruction was based on defining a pattern of a network of images with baselines, which must ensure adequate levels of overlap. This aspect is influenced by the resolution of the images, the angle of photographic capture, and the mutual distance between images, and it influences the quality of 3D reconstruction. Scanning based on SfM-MVS allows dense point clouds to be obtained with the use of uncalibrated perspective and spherical digital cameras with very good quality color data. In our case, we used a specific digital camera with an APS-C sensor that has a dynamic range value of 13.7 EV (>12EV high-quality limit) and excellent noise performance values at high and low sensitivity and color depth. The shape and size characteristics of the monument for both outdoor and indoor scenes required the combined use of different UAV and ground-based image acquisition techniques and materialized GCPs and CPs control points with encoded targets. The distribution of GCPs and CPs was based on the topography terrain characteristics of the area and those of the still outcropping structures of the monument. The identification of GCPs is related to image resolution and GSD. GCPs can be identified by encoded targets but also on natural objects that must be identifiable in images with resolution consistent with the GSD value used [26]. Several models of codified targets have been proposed in the literature, which must be clearly distinguished from each other and have a robust disambiguation with environmental characteristics. Ground-coded targets were accurately identified through automated procedures in the photogrammetric georeferencing process of the project coordinate system. In general, coded targets can be classified into three categories: 1D targets, planar targets, and 3D targets [33]. In our study, planar targets were chosen with patterns of concentric circles and black circular dots of the Schneider type and black and white patterns arranged within square frames, generated through QR codes of the AprilTags type [34]. Schneider targets were used for nadiral and oblique converging surveys performed with UAVs and AprilTags targets for the survey of entrances and internal parts of the monument. Schneider-type targets have a simple geometry that makes them more robust in low-light and low-resolution conditions than targets with more complex patterns. Moreover, the perspective deformation of the concentric shape means that the projection of the circles into ellipses with increasing distance does not compromise recognition in space [33,34]. AprilTags targets are designed to be easily identified and decoded by computer vision algorithms due to the strong contrast and well-defined edges that allow robust detection even in limited lighting conditions. To correctly reconstruct the relationship between the 2D coordinates of each image and the coordinates in 3D space, the automatic identification of the measurement points, on the basis of the points of the image, is essential [32,33]. The targets used in the present study have dimensions of 29 × 29 cm and 15 × 15 cm and were printed on rigid supports carefully positioned on the points on the ground. With the use of these targets, the process was accelerated, improving the accuracy and reliability of the measurements on the 3D model. GCPs and CPs have been materialized both as reference vertices, through coded artificial targets, and as natural feature points on the ground or structure in question (Figure 3). The network of GCPs and CPs points was measured with GNSS (global navigation satellite system) real-time kinematic (RTK) techniques using a Topcon Corporation (Tokyo, Japan) Legacy-Hyper V5 receiver in RTK mode. GCPs and CPs were measured using a rover and GPS base station. The rover antenna was set to PDOP = 4.0, and horizontal and vertical precision tolerances were set to 0.010 m + 1 ppm and 0.015 m + 1 ppm, respectively, while the base was set to have a 15° elevation mask. The base station used for RTK-GNSS surveying recorded for a time of 1 h on a point of known coordinates. The accuracy level of the base station was 0.01 m in the vertical and horizontal components. With the rover

antenna, data were recorded for each GCP and CP for 5 min. The accuracy of the kinematic method allowed for centimeter-level accuracy.

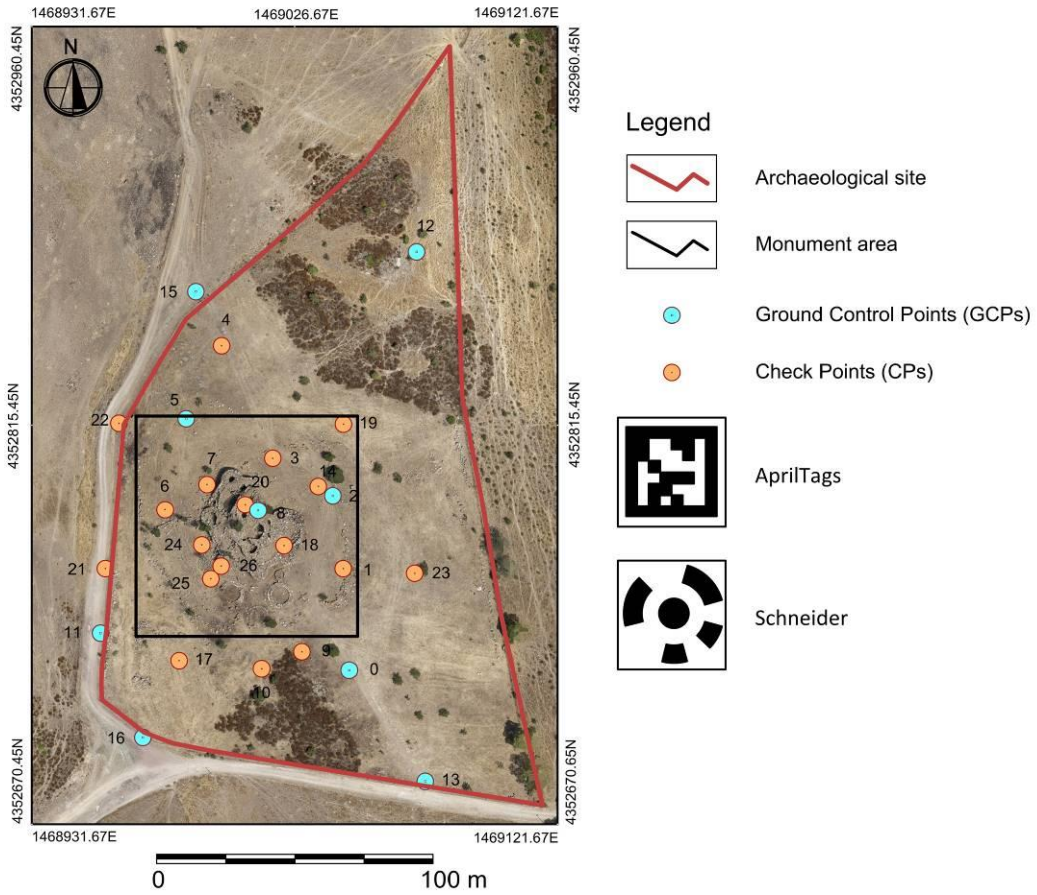

Figure 3. Spatial distribution of ground control points (GCPs) and check points (CPs) and target types used in photogrammetric survey.

Using a series of oblique convergent images, it is possible to reduce systematic error in stereo pairs acquired with linear UAV flight patterns. Therefore, by integrating nadiral acquisition with convergent acquisition, as demonstrated by several studies, systematic deformation can be effectively reduced [23]. The parameter that most influences the accuracy of a photogrammetric model is the base-to-height ratio (B/H) [28]. For nadiral photogrammetry, the optimal B/H ratio can vary according to the geometry of the object or scene and is in the range of $0.2 \leq B/H \leq 0.4$; for convergent photogrammetry, the optimal B/H ratio, which can also vary according to the geometry at the shooting angle, is in the range of $0.1 \leq B/H \leq 0.5$ [24,25]. Several studies have shown that for vegetation-free soil types and grass-covered areas, measurements from multiple stereo pairs are quite consistent with an advantage to DSM accuracy. In the case of areas covered by high vegetation, the dispersion of the elevation data from stereo pairs is significantly greater. The quality of the elevation measurement is highly dependent on the B/H ratio and the type of ground cover. On flat areas of vegetation-free terrain, elevation assumptions from high B/H ratio stereo pairs are more consistent. On the other hand, in areas with vegetation, most assumptions of elevation from high B/H ratio stereo pairs are anomalous [37]. Elevation data from stereo pairs with lower B/H ratios generally better represent the ground surface and, importantly, contain significantly fewer outliers. This is because nearby images are more similar to each other and, therefore, searching for matches is more efficient. Elevation data from stereo pairs with the lowest B/H ratios allow for a first approximation of the reconstructed surface [37].

2.4. 3D Modelling

The reality capture software (RC) [31] uses an evolution of sophisticated algorithms for Multi-View Stereo Reconstruction (MVS) and allows for the management of large amounts of data to obtain high processing speeds, to guarantee reliability, and to extract highly structured surfaces, as demonstrated by several authors [17,24,25,38,39]. It allows for automatic classification through artificial intelligence (AI classification on DSM), editing interventions with semi-automatic procedures on 3D models and textures. AI classification can allow for the creation of ortho-views, cross-sections, and measurements extrapolated directly from 3D models. It enables the definition of standardized and repeatable workflows. The workstation used for processing was a QuadCore Intel Core i7-4820K (8 Mb Cache) 3700 MHz CPU with 64 GB of DDR3-1333 MHz RAM and an NVIDIA GTX 1080 Ti GPU with 11 GB GDDR5X. In RC, multiple RRs have been defined for each survey area to limit the reconstruction of 3D space. We have defined RR_1 for the survey area for topographic mapping with an extension of 190 × 290 × 32 m and RR_2 for the monument area with an extension of 80 × 80 × 18 m. The relief area of the RR_2 monument area has been divided, as described above, into external and internal scenes. A further RR_3 region with an extension of 48 × 45 × 18 m has been defined to elaborate the ortho-views and characteristic sections of the Nuraghe. The use of reconstruction regions makes it possible to optimize the photogrammetric calculation process and to focus dimensional and accuracy analyses at the local scale on parts of the monument of particular interest. Multiple RR reconstruction regions allow for the optimization of the reconstruction of specific parts of the scene, speeding up the photogrammetric process and improving the quality of processing. Each region can be moved, rotated, and resized via the RC widget. The reconstruction regions defined in the project can be exported and imported to other platforms (CAD, GIS) to generate 3D sub-models, ortho-views, and ortho-sections on specific areas of interest of the 3D model.

2.5. Accuracy Assessment

The level of accuracy and visual quality required in the final 3D model and the quality constraint required to validate the geometry of the SfM-MVS 3D model were established with a maximum allowable error of <=2.5 cm. For this purpose, the georeferencing accuracy was evaluated on the basis of the estimation of the X,Y,Z residuals of the GCPs calculated from the RTK-GNSS measurements. The rigidity of the 3D model influencing the propagation of errors in space was evaluated through the estimation of the errors of the Euclidean reciprocal distances of the GCPs and CPs with a comparison between the calculated and measured data. The error of coherence and geometric completeness of the surface reconstruction was estimated with a cloud-to-cloud distance (C2C) using Cloud Compare software (CC) Version 2.12.4 [40] through a comparison between the sample surfaces processed from images acquired with the same APS-C sensor as that used on the typical surfaces of the SfM-MVS 3D model. Finally, an analysis of the completeness and visual quality of the texture of the reconstructed surfaces was carried out. The positioning accuracy of a 3D model was evaluated by calculating the mean (MEAN), standard deviation (STD), mean absolute error (MAE), and root mean squared error (RMSE) of the residuals on the GCPs (9) and CPs (18) using the coordinates measured on the ground with the global positioning system (RTK-GNSS) and those calculated using the photogrammetric model [28,32]. To evaluate the global geometric rigidity of the SfM-MVS 3D, the Euclidean distances of a 3D Delaunay network defined using GCPs and CPs were compared with those measured using RTK-GNSS at the site for the estimation of the RMSE value [17]. The evaluation of the quality and completeness of the SFM-MVS 3D model at the local level was based on the assessment of the error of the mesh vertices with a direct comparison between a generated point cloud and a ground truth reference point cloud. TLS scanning is widely used in the documentation of architectural heritage and allows data to be acquired with millimeter-level precision for 3D modelling. Several studies have verified the performance of SfM-MVS models obtained using full-frame DSLR sensors compared

to a reference "ground truth" benchmark acquired using a terrestrial laser scanner (TLS). For full-frame DSLR sensors, C2C errors < 0.5 cm with 95% confidence and RMSE on Euclidean distances of <0.8 cm compared to the laser scanner [17] were obtained. For the APS-C sensor, we repeated the tests performed on surface types with "ground truth" benchmark comparison with the Faro Scene 350 at distances of 5 and 10 m. This laser scanner (Class 1, λ = 1550 nm) has a measurement error of $\pm$1 mm and an accuracy in detecting 3D positions of 2 mm at $\pm$ 10 m and 3.5 mm at 25 m; for longer distances, the accuracy decreases in increments of 0.1 mm per meter. C2C errors of <0.7 cm with 95% confidence and RMSEs on Euclidean distances of <0.9 cm were obtained. The C2C error is about 1/1000 of the maximum measured width, and it shows good overall accuracy of the photogrammetry model compared to the reference laser scanner. In our study, the quality of the reconstruction in terms of surface deviation was evaluated on typical surfaces of the Nuraghe, using our APS-C sensor mounted on tripods and telescopic masts, to obtain a comparison based on a benchmark "ground truth" positioned at 5 m from walls. The aim was to verify whether the quality of the reconstruction from the APS-C camera could be consistent in terms of geometry and texture quality with the requirements of the proposed photogrammetric workflow. The use of the same sensor has the advantage of having the same internal acquisition geometry, the absence of systematic distortions due to the use of different sensors, and a direct comparison between the "ground truth" and the SfM-MVS 3D model. Each benchmark was defined by ratio of 1:10 between the GSD of the photogrammetric survey and that of the "ground truth", which is largely sufficient to perform a reliable analysis of geometric deviations in surfaces. In case the GSD survey for some walls is lower than or equal to the GSD benchmark, it is possible to exclude these areas from the C2C validation, as the resolution of the photogrammetric model is already higher than or equivalent to the "ground truth". The surfaces selected as typical have covered a variety of shapes of walls, materials, and textures present, so that a meaningful assessment of model completeness could be obtained. The datasets acquired for each typical surface were aligned in the SFM phase with the survey data to then calculate the individual "ground truth" MVS models for the C2C validation. The following is given as an example of a photogrammetric benchmark performed on a typical surface represented by the external face of the M tower, which develops on the XY and XZ planes, delimited by the RR_4 reconstruction region with a size of 12 $\times$ 4 $\times$ 5 m. This process employed the use of a tripod/mast, remote control shooting, constant light conditions, and specific base/height (B/H) ratios, ensuring optimal baseline configuration. The capture GSD was 0.13 cm/pixel (camera–object distance = 5 m). The M1 "ground truth" model was calculated in RC with 1 cm spacing. In the same way, the M2 "flight and ground survey" model was calculated in RC, delimited by the RR4 with a spacing of 1 cm with an average GSD from the overall survey equal to 0.54 cm/pixel (camera–object distance settings varying in the ranges of $5 \leq D \leq 50$ m for the external scene and $1 \leq D \leq 5$ m for the internal and access scenes). The validation of the M2 model was performed using the cloud-to-cloud distance C2C (M1–M2) comparison based on the Hausdorff distance between point clouds with 99% outlier elimination. This validation also included an analysis of the completeness and visual quality of the texture of the reconstructed surfaces.

2.6. Characterization of Building Materials and Geoarchaeological Investigation

A typological evaluation of the nature of building materials used for the construction of the monument was based on a sampling of the stone ashlars and the filling material of the masonry structures, carried out in compliance with the visual integrity of the Nuraghe. The sampling was also extended to the geological outcrops present in the archaeological area. On these outcrops, a survey of the layering parameters was also carried out to correctly report the trend of the geological substrate in the elaboration of the geological map of the archaeological site. For the sampling, to define the compositional characteristics of the investigated materials, XRD mineralogical analysis was performed using a Rigaku Corporation (Tokyo, Japan) Geigerflex D-Max/B X-ray diffractometer with a Cu anode, operating at

30 kV and 30 mA. On the basis of the results obtained in this phase, a geoarchaeological survey was planned beyond the limits of the archaeological site in order to verify the presence of geomaterials compatible with those used for the construction of the Nuraghe. During this survey, several stone blocks present in the slope deposits around Mt. Acqua and from alluvial deposits in the Rio San Giovanni valley were sampled and analyzed. Finally, the mineralogical characteristics of the monument sampling were compared with those of the geomaterials present in the investigated area to verify compatibility and identify possible places that supplied the stone used in the Nuraghe.

3. Results

3.1. Geological Investigation on Building Materials

The archaeological site is an area that is mainly characterized by geological outcrops attributed to the Paleozoic basement of Sardinia (Figures 4 and 5). In particular, the monument rests on metamorphic outcrops consisting of metasiltstones, metapelites, and subordinated quartzites, referring to the Medau Murtas Member of the Medau Argentu Formation (middle-upper Ordovician ?; [41]).

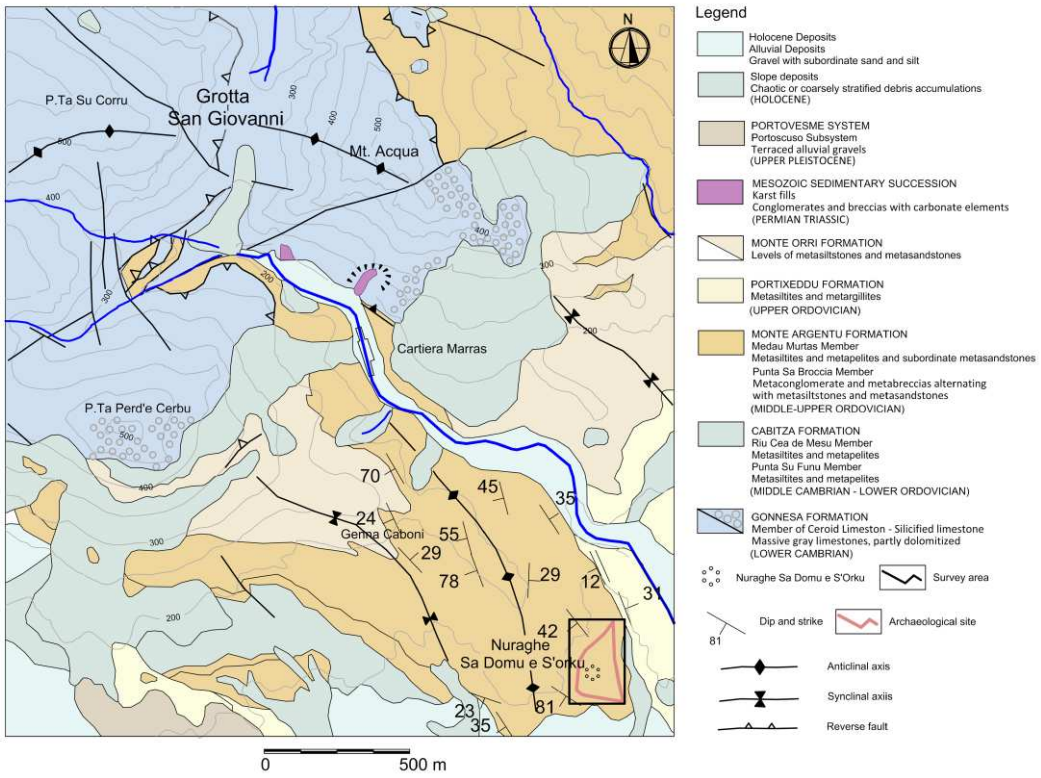

Figure 4. Geolithological sketch map of the studied area.

Outside the limits of the actual archaeological site, in the northern direction, the territory is dominated by limestone outcrops attributed to the Calcare Ceroide Member of the Gonnesa Formation, which constitutes the reliefs of Mount Acqua, Punta Su Corru, and Punta Perd'e Cerbu (Lower Cambrian; [41]). A substantial portion of these outcrops has undergone a profound phenomenon of silicification that has led to the complete transformation of the original limestones. This silicification has particularly affected the southeastern side of Mt. Acqua and the southern part of Punta Perd'e Cerbu. Substantial deposits of these silicified materials were found on the slopes of Mount Acqua and in the riverbed of the Rio San Giovanni in the form of flat or cuneiform parallelepiped blocks, variously elaborated, ranging in size from 0.5 m to 2 m (Figure 6).

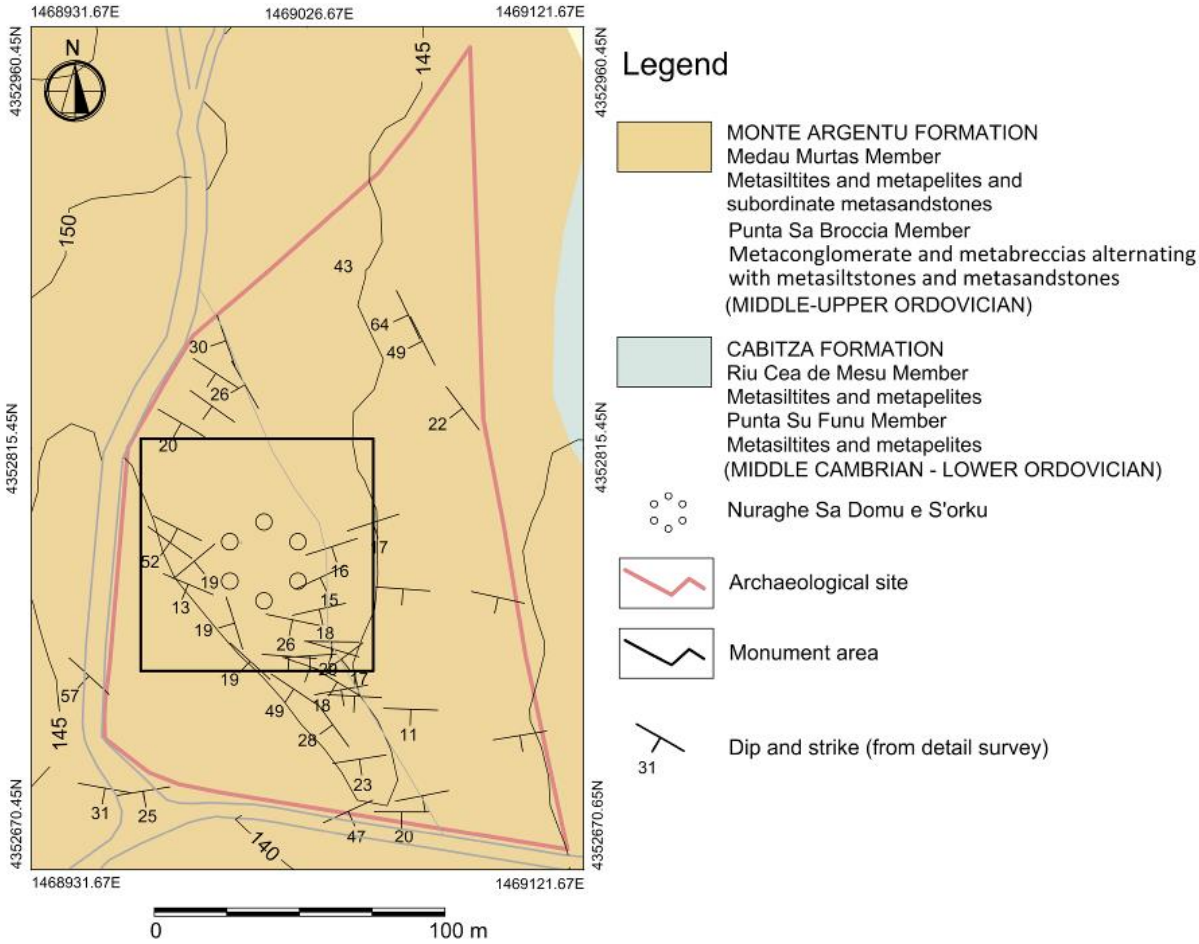

Figure 5. Geological sketch map of archaeological site. Ground points measured by RTK-GNSS on geological outcrops to estimate the elevation at the base of the Nuraghe.

Figure 6. (**a**) Blocks deposited along the valley of the Rio San Giovanni containing breccias; (**b**) partially elaborated silicified blocks coming from the slopes of Mt. Acqua.

As described in the previous section, the characteristics of building materials used in the structures of the Nuragic site were defined starting from their typological characterization based on macroscopic observations and then more deeply through XRD analysis (Figures 7 and 8). This highlighted the prevalent use of fully silicified lithologies. Given their composition, stone ashlars are extremely tough and appear unshaped or slightly hewn and laid dry (without mortar) according to a complex polygonal pattern of joints. Alternatively, there are small- and medium-sized blocks of metapelite and metasiltstone, used mainly to fill the voids and hold the larger elements of the masonry in place. In the partially collapsed structures, it is possible to observe the masonry construction technique, characterized by two faces, consisting of blocks inclined toward the inside and opposed to each other, whose major axis is at least 2/3 inside the masonry itself. The dry masonry always contains a variable amount of compacted filling material between the two facings, consisting of stone fragments with an average size in the decimetric range, immersed in a matrix with gravelly, sandy grain size. The results of the analyses on the samples taken during the geoarchaeological investigation showed a marked similarity in compositional and morphological characteristics between the stone blocks in place in the wall structures of the Nuraghe and the coarser elements of the deposits present in large quantities in the valley of the Rio San Giovanni and on the slopes of Mt. Acqua.

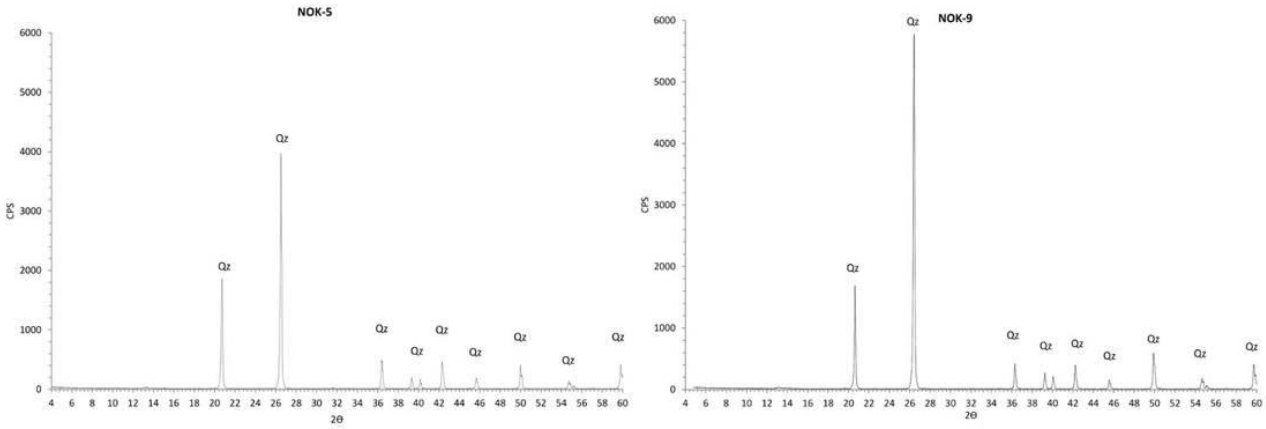

Figure 7. XRD analysis of stone blocks from the Nuraghe and comparable geomaterials of the investigated area. NOK-5 sample from main tower wall; NOK-9 sample of silicified stone block from stratified slope deposits of Mount Acqua. Qz = quartz.

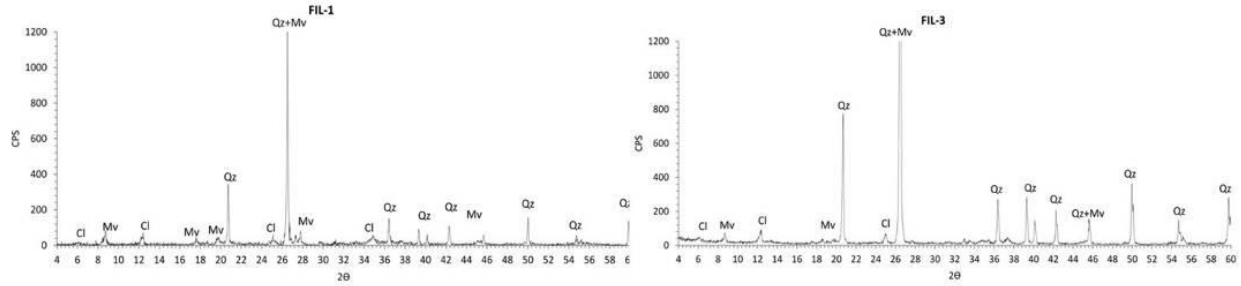

Figure 8. XRD analysis of filling material from the inside part of the masonry and compatible material from the riverbed of the Rio San Giovanni. FIL-1 sample from the inside of the rampart; FIL-3 sample from riverbed deposit. Qz = quartz; Mu = muscovite; Cl = chlorite.

The filling material inside the walls is also compatible with local colluvial deposits and sandy and gravelly deposits along the valley and in the bed of the Rio San Giovanni, derived from the erosion and transport of metamorphic basement rocks. Among the elements of the filling material in the walls of the Nuraghe, we found large amounts of refined metasiltstone and metapelite pebbles immersed in a sandy–silty fraction that show the same mineralogical composition as these metamorphic lithologies. The presence of refined pebbles leads to the reasonable hypothesis that these sandy–gravelly fractions came from the river deposits of the Rio San Giovanni.

The definition of the typological characteristics of the geological materials used for the construction of the Nuraghe and the attribution of the areas of origin are decisive in enriching the knowledge of the technological level reached by the Nuragic civilization.

The contribution of the laboratory analyses and the geological survey of the area confirm these data objectively, allowing for the verification of the preliminary classification of building materials performed on an autoptic basis. In addition, it has been pointed out that the mineral–petrographic characteristics of the stone material denote its particular hardness and the objective difficulty to model the blocks into regular shapes with the tools available at the time. However, this apparent limitation did not prevent the Nuragic builders from creating a complex monument, characterized by the careful selection of the shapes and sizes of blocks found in natural deposits. The decision to use predominantly silicified materials (consisting, as demonstrated, of pure quartz) for the Nuraghe blocks, rather than the limestones widely available in the region, is likely related both to their great availability in the proximities of protohistoric settlement and to their greater durability and resistance over time.

3.2. 3D Modelling of the Nuraghe

The 3D reconstruction workflow used in the reality capture software (RC) included the image alignment based on GCPs and CPs, SFM sparse point cloud reconstruction, and dense MVS (Table 2).

Table 2. Advanced alignment parameters in reality capture.

Alignment Parameters	Value
Alignment mode	High
Max features per Mpix	10,000
Max features per images	40,000
Detector sensitivity	High
Preselector feature	20,000
Image download factor for depth maps	1
Max feature reprojection error (pix)	1
Lens distortion model	K + Brown 3 with tangential 2
Alignment time	02 h:19 m:25 s
Feature detection time	00 h:26 m:41 s
Registration time	01 h:52 m:43 s
Maximal error (pix)	0.999999
Median reprojection error (pix)	0.336809
Mean reprojection error (pix)	0.381691
Camera count	3459
Point count	7,845,986
Control point used	9(GCPs) + 18(CPs)
Background thread priority	Normal

Next, the cleaning and topology of the 3D model, mesh texturing and simplification, 3D tiling, and the creation of sub-models for each defined reconstruction region were performed. Finally, the accuracy of the 3D model was evaluated and exported for further processing. In RC, the design coordinate reference system was EPSG:3003. For the SfM alignment process, the distortion model "K + Brown 3 with tangential 2" was used, and then the positions of the cameras were obtained and the sparse point cloud computed. In the subsequent phase, MVS computed the dense point cloud that was restricted to the reconstruction region RR_1 and RR_2, with a minimum spacing of 1 cm. RC reconstruction was performed in "High" mode, with an image resize factor for depth maps set to 1. The mesh model was calculated from the dense point cloud (Table 3). The model was cropped, simplified, re-textured, and exported as a point cloud in the .xyz and mesh format .obj to complete the dimensional survey and 3D visualization. The next phase of model simplification focused on consistently maintaining the original geometry in shape and size for each region of reconstruction RR model. This was performed in relation to the best ratio between the reduction in triangle area and the conservation of the quality of geometric representation. In RC, by adjusting the simplification parameters, it was possible to achieve a good compromise between the simplification and preservation of the original geometry, in order to preserve the mesh connectivity, the original topology, the edges, and the salient characteristics of the key vertex, avoiding even a partial collapse of regions. For validation, 3D metrics were used between key points, and cloud-to-cloud Hausdorff distance C2C comparison was used between original and simplified mesh. This phase resulted in simplified 3D models for each reconstruction region with a minimum edge length of >1 cm, consistent with the maximum constraint error. The reprocessing of the textures from the original models to the simplified ones has preserved the overall visual quality of the 3D reconstruction.

Table 3. Advanced reconstruction parameters in reality capture.

Reconstruction Parameters	Value	Value
Reconstruction region	RR_1	RR_2
Dimensions L × l (m)	290 × 190	80 × 80
Quality level	High	
Minimal distance between two vertices (m)	0.01	
Triangle count	372.8 M	109.6 M
Vertex count	187.0 M	55.0 M
Depth-map computation time	05 h:35 m:10 s	04 h:39 m:57 s
Meshing time	15 h:37 m:40 s	09 h:52 m:50 s
Overall processing time	21 h:12 m:50 s	14 h:32 m:47 s

The SfM-MVS 3D model of the monument allowed for the evaluation of the above-ground volumes to define the proportions of the collapsed and covered parts and to formulate hypotheses about the original dimensions of the Nuraghe. The 3D model reproduces a "Digital Twin" of a "complex Nuraghe", with a floor plan illustrating a main tower, a rampart with a polylobate structure surrounded entirely by walls and five perimeter towers. The representation scale of the 2D and 3D drawings was 1:100 for ortho-views and 1:500 for ortho-photos and DSM, with the maximum allowable error congruent with the desired level of detail <= 2.5 cm (Figures 9 and 10). This value was the quality constraint to validate the geometry of the SfM-MVS 3D model.

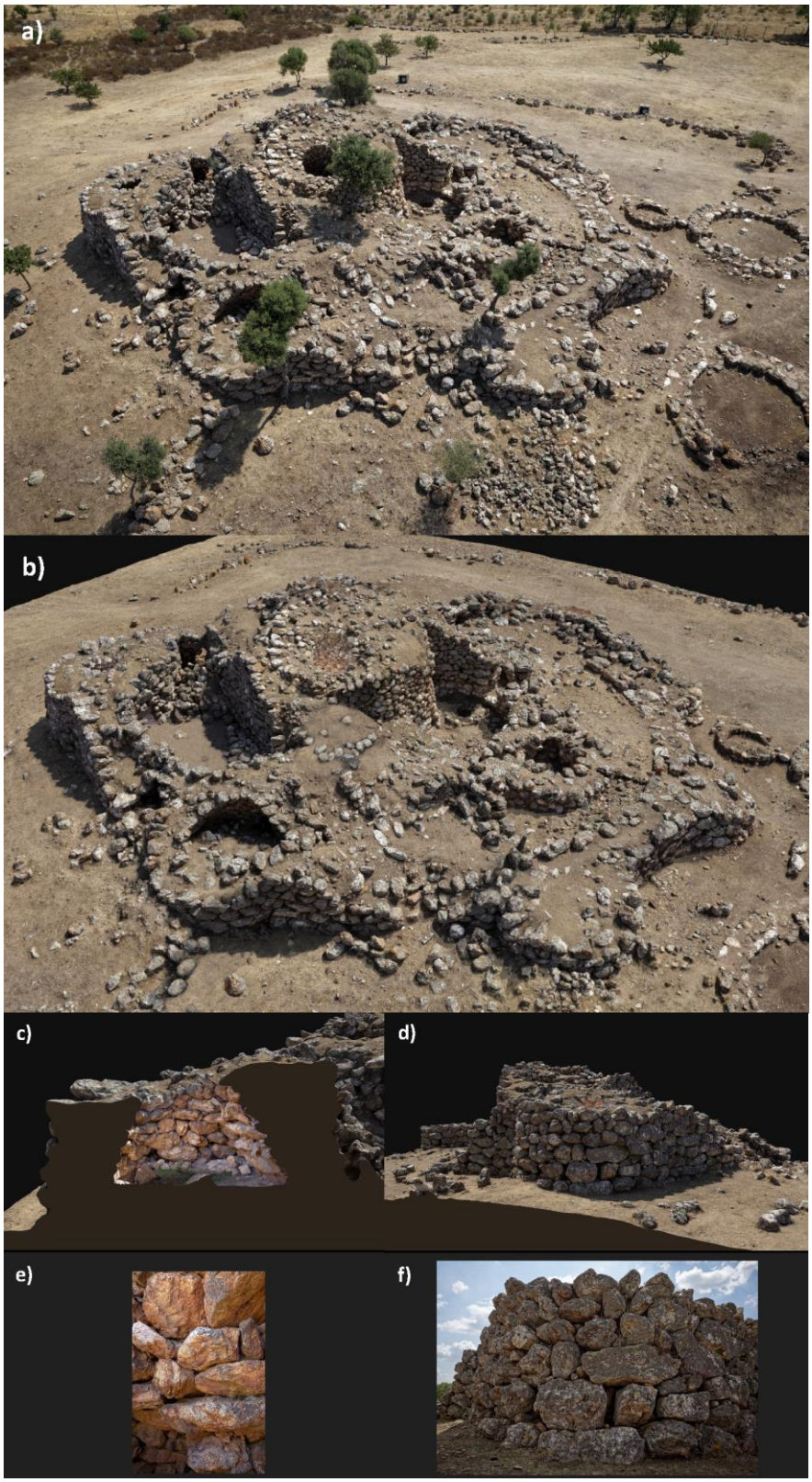

Figure 9. (**a**) Aerial photo of the Nuraghe (SW–NE); (**b**) view of the optimized 3D model of the Nuraghe in RC according to the reconstruction region defined for the monument area under survey (SW–NE); (**c**,**d**) views of the textured mesh of internal chamber and external walls; (**e**,**f**) example photos of internal chamber and external walls.

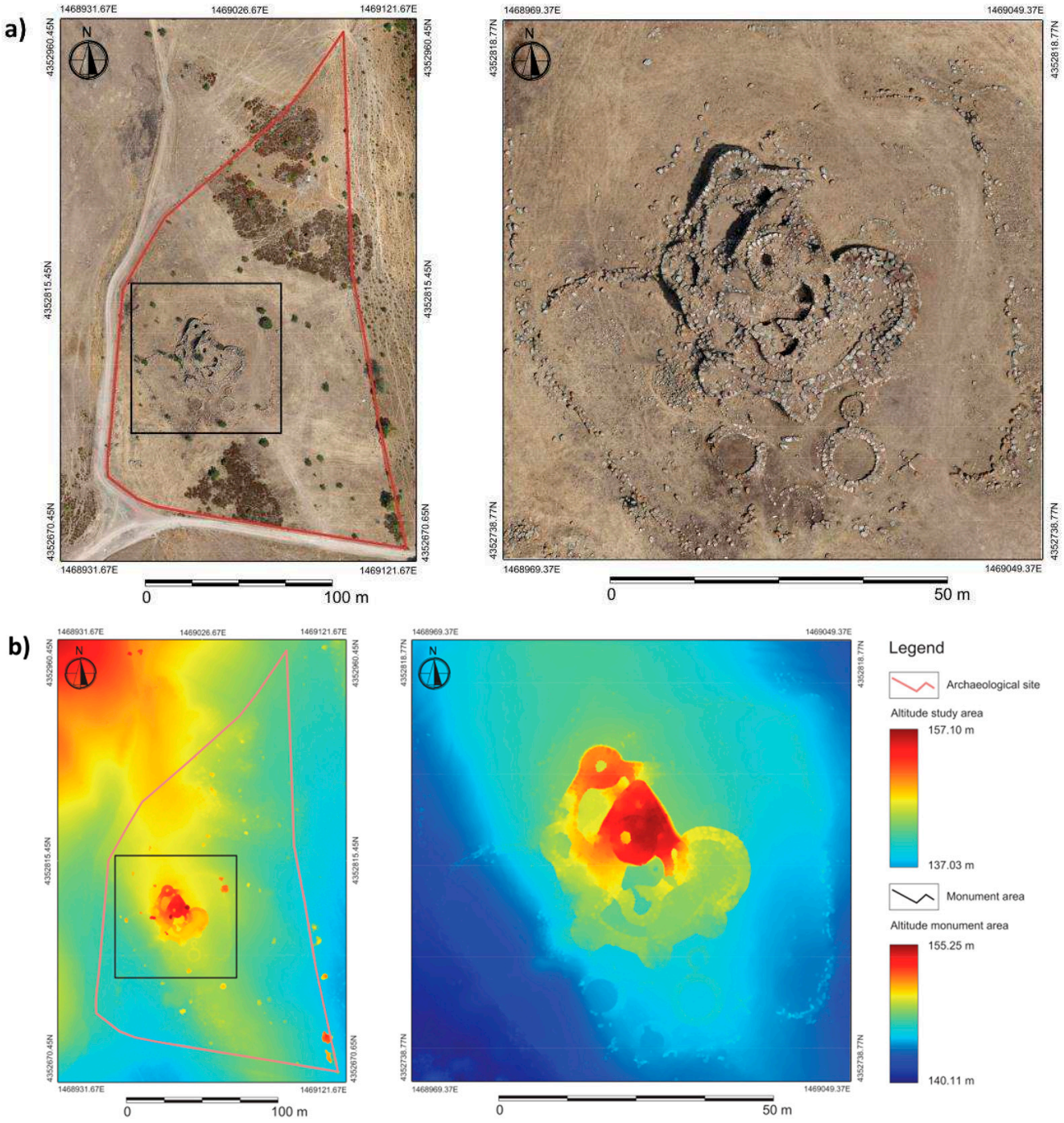

Figure 10. (**a**) Ortho-photo of photogrammetric survey area and monument area (left); (**b**) DSMs of archaeological site.

The hypothesis of the original proportions of the monument, based on previous observations of this Nuraghe and similar structures [1,3,8–11], was tested also through a purely geometric approach, based on the relationships between dimensions of diameters, angles, and profiles of the above-ground structures from the sections calculated from the SfM-MVS 3D model. The dimensional ratios and shapes typical of Nuragic structures were estimated, such as the height/diameter (H/D) ratio of the towers and their tholos chambers. Hypotheses were made to complete the profiles of the best fit of these chambers starting from characteristic points identified in the type sections. Proportionality and the integration of the missing parts were applied based on existing structures. The consistency of the

estimated proportions with the geometrical constraints compatible with the still-accessible structures was verified. Particular attention was paid to the height of the access openings to the Nuragic towers and to the perimetral walls to define the lower levels of the entrances to complete the TIN of the rocky outcrops at the foundation of the Nuraghe. By processing in a CAD environment with parametric algorithms, it was possible to define a 3D Delaunay triangulation of the ground points detected on geological outcrops to define the share of the foundation base of the Nuraghe and to identify some 2D geometric descriptors of the structure from the characteristic sections. This allows for the reconstruction of 3D geometries for extrusion and the representation of the original dimensions and proportions of the monument based on the currently accessible measures of heights and wall thicknesses. Parametric processing with CAD on the 3D SfM-MVS model of the structures allowed for the definition of the original elementary volumes using interpolated lines and curves and the TIN model of the ground on which the monument rests as a basis. Using CAD tools for parametric 3D modelling, from basic 2D geometries, it was possible to obtain 3D models reconstructed according to the original proportions data. The maximum height for the towers was estimated starting from the constraints defined by the external basic dimensions and tholos chambers, the inclination of the external wall profiles, and the estimated shape and height of the internal elliptical paraboloid profile of the chamber. The strategy in use is based on the progressive calculation of the reduction upwards of the tower section and the wall thickness as a function of the inclinations of the two sides. In this way, it was possible to estimate the maximum height beyond which it is no longer possible to continue due to geometric limitations related to the wall thickness, the variability in the shape and dimensions of the blocks, and the maximum height of the inside profile. The maximum height of the tower was hypothesized based on the height constraint established according to the profile of the tholos chamber and the assumed thickness of the roofing material placed on its top. The construction solution adopted in the Nuraghe investigated involved the use of stone blocks that were irregular and polyhedral wedge-shaped, arranged to obtain walls that were perfectly aligned according to a precise inclination. The choice of wedge and flat shape is effective both for the towers of circular section, where the internal and external radius of curvature are concentric, and for open and closed polylines (as for the bastion and the perimetral walls), where it offers good adaptability in areas with a strong convergence of structures as a function of variability in wall thickness and inclination. Through the analysis of the 3D model SfM-MVS, all the information was obtained to formulate a geometric hypothesis that allows for the reconstruction of the missing parts, according to the construction rules typical of Nuragic structures. This approach allowed for the proposal of the maximum height of the towers, of the bastion, and of the perimetral walls and the evaluation of their reciprocal proportions. Area, volume, and other measurements on the 3D model were made directly in reality capture (RC) and in a CAD environment.

Studies in this field often report indications on the architectural proportions of Nuraghes, indicating the main sizes and significant dimensional parameters used to describe and compare structures and understand the variety of Nuragic architecture according to types and construction techniques. However, dimensional parameters are often presented in descriptive and qualitative terms, without a systematic analysis of ratios and proportions between architectural elements [12]. In this study, geometric parameters were systematically detected and measured. According to Vanzetti et al. [12], the main measured quantities and significant dimensional parameters to describe Nuragic structures are as follows:

- Height of the tower (H): a fundamental measure to quantify the overall dimensions of the Nuraghe. Variability from a few meters up to about 20 m.
- Diameter of the tower (D): indicates the width of the building base. Usually in the range of $10 \leq D \leq 20$ m in larger Nuraghes.
- Number of towers: indicates the degree of articulation of the structure in complex Nuraghes.
- Presence of walls: particularly in complex Nuraghes.

- Wall thickness: construction scheme with double side, with intramural space that can reach several meters in the most imposing Nuraghes, giving stability to the structure.
- Dimensions of the internal chambers: diameter (d) from 3 m up to about 6 m and height (h) from 3 m to about 8 m are key parameters to evaluate the organization of the interior spaces.
- Dimensions of openings and corridors: indicate the width of the passage points in the structure.
- Materials, dimensions, and shape of boulders: length, width, and thickness recurring in erratic boulders as well as their shape and physical characteristics in terms of workability are an index of construction capabilities.

Below is a report of the main dimensions measured in the Nuraghe studied. The towers indicated in Figures 11–13 with A, M, G, H, I, and L have a truncated cone shape with heights above ground between 2.10 and 7.00 m and total heights estimated between 5.50 and 14.30 m.

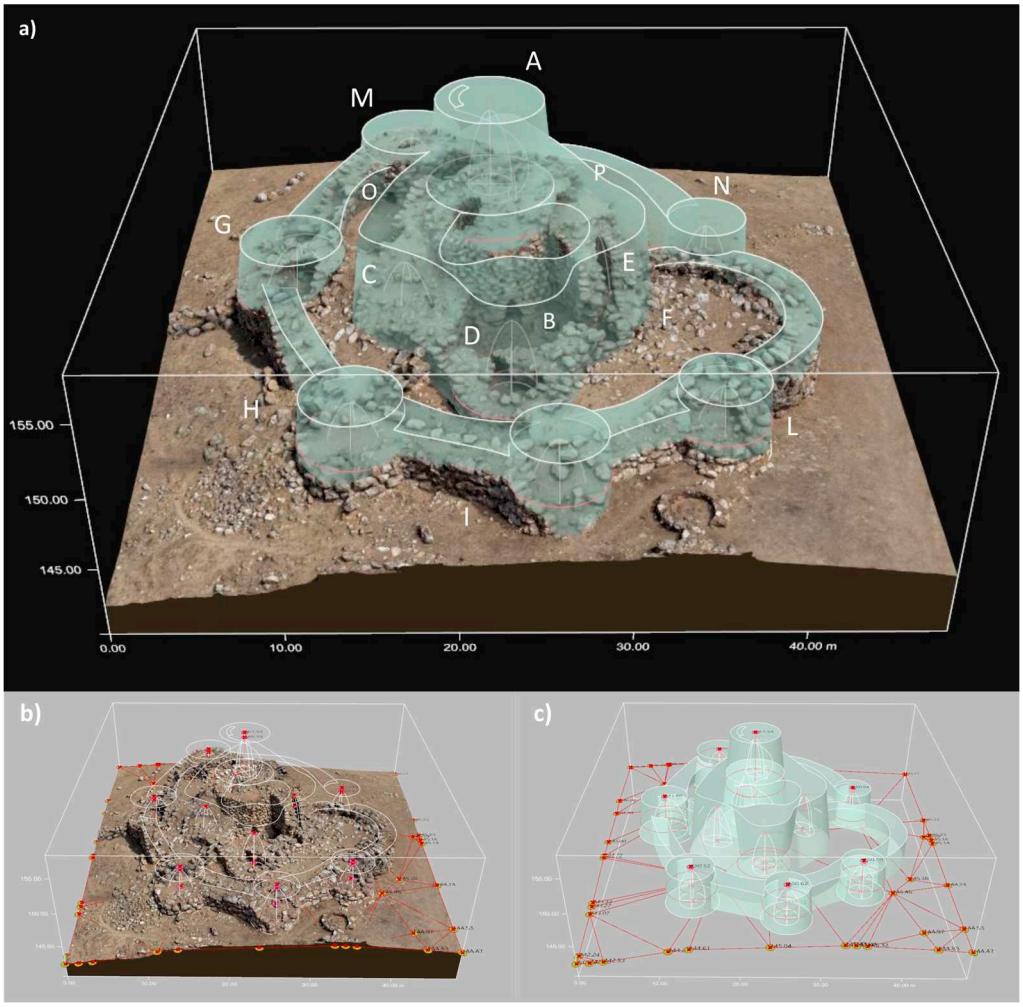

Figure 11. (**a**–**c**) 3D reconstruction of the Nuraghe with visualization of the missing parts (RR_3) obtained on the TIN foundation base of the Nuraghe. The different parts of the monument (from A to P) are described in the paragraph below. The approach used allowed for the estimation of the maximum height and the definition of the proportions between towers, ramparts, and perimeter walls.

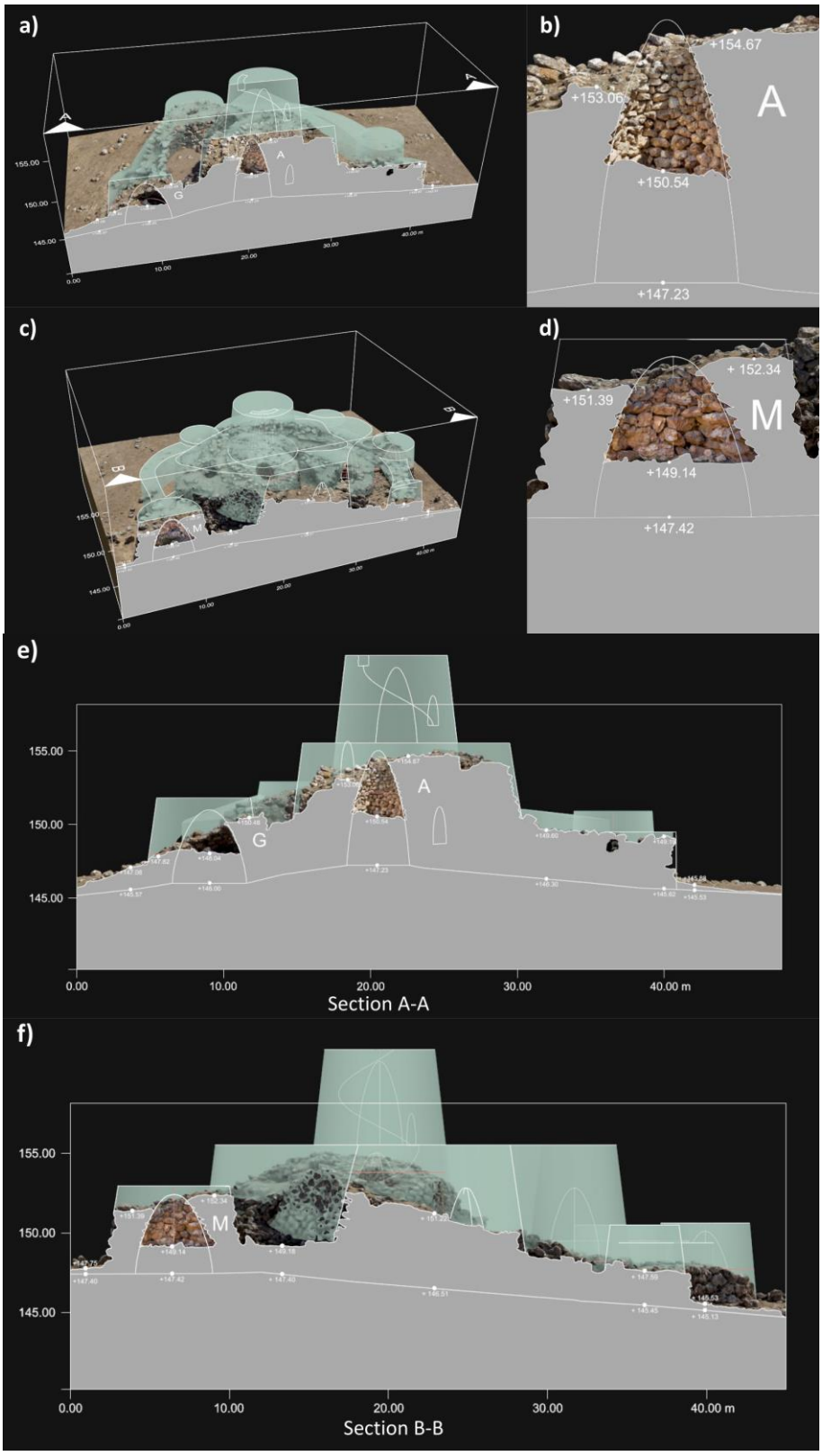

Figure 12. 3D model of the Nuraghe and hypothesis of reconstruction of the original dimensions of the monument. (**a**,**c**,**e**,**f**) Perspective and orthostatic view of sections A-A and B-B; (**b**,**d**) simplified 3D model: detail of the tholos of towers A and M.

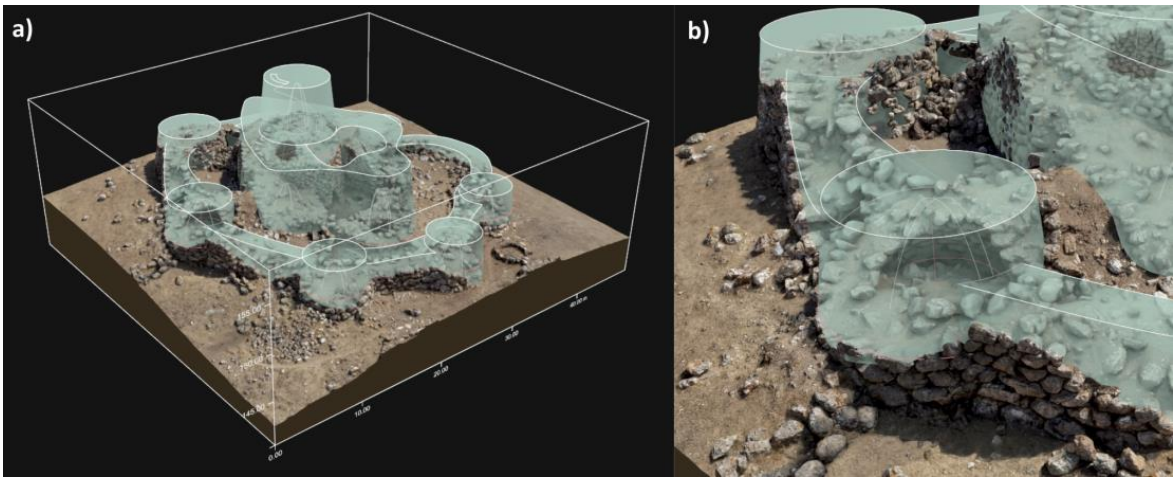

Figure 13. 3D model of the Nuraghe and reconstruction of the original proportions of the monument. (**a**) Perspective view; (**b**) detailed view.

The estimated base diameters vary from 6.10 to 10.20 m, and the top diameters vary from 5.40 to 7.00 m. The average slopes are between 4.0° and 8.65°. H/D ratios are between 0.63 and 1.40. The internal tholos chambers have circular or elliptical base shapes, with estimated heights of 4.84 to 7.80 m and average diameters of approximately 3.10 to 5.30 m. h/d ratios are in the range of 1–1.47. The estimated surface walls of the tholos chambers are elliptical paraboloid. The main tholos A has an elliptical base with axes of 5.30 m and 4.30 m and an estimated height of 7.80 m. At the upper level, the second tholos is presumed to have a circular base of 2.87 m in diameter and 5.25 m in height. The minimum thickness above the tholos chambers is established as >0.50m. The wall thickness, off-center location, and size of the tholos on both levels of Tower A are geometrically consistent with the hypothesis of the existence of a connecting staircase with helical development. This, as evidenced by previous studies [1], starts from the right side of the access corridor and likely reaches the top of the tower [10,11]. The ratios between the diameter of the tower and the diameter of the tholos chamber (D/d) are between 1.55 and 2.10. The axis of the access corridor to the main tower is oriented N154° E. Access exposure is in the SE quadrant. The maximum dimensions of the blocks of the load-bearing structures are in the order of 1.40–1.80 m in width, 0.70–1.00 m in height, and 0.90–1.20 m in thickness. The minimum dimensions are 0.40–0.60 m in width, 0.35–0.50 m in height, and 0.60–0.80 m in thickness. The tholos blocks have minimum dimensions of 0.4–0.5 m in width, 0.30–0.35 m in height, and 0.50–0.70 m in thickness. Tower N and part of the east perimeter wall were assumed to exist based on earlier indications found in other studies [1,10,11]. The rampart has a polylobate structure and a current height above the ground of 7.40 m, while the original height is estimated to be 8.40 m. The outer wall side has an average slope of 6.95°. Although not perfectly visible and measurable, two other possible chambers D and E are identified in the Nuraghe. A tholos with a circular base of 3.20 m diameter and a height of 5.65 m, defined according to an h/d ratio of 1.76, is assumed for chamber D. The tholos of chamber E has the same height as the previous one and an elliptical base with axes of 4.30 m and 3.10 m, from which an average h/d ratio of 1.31 is derived. The estimated surface wall of the tholos chambers is an elliptical paraboloid. The area of the internal courtyard B is approximately 30 m^2, while the footprint of the keep is 315 m^2. The lateral tholos chamber C to the west was hypothesized on the basis of estimates of the proportions of the chambers and previous indications made by other studies [1,10,11]. The maximum dimensions of the blocks at the base are 0.90 m width, 0.70 m height, and 0.95 m thickness, and the minimum dimensions are 0.60 m width, 0.40 m height, and 0.70 m in thickness. The perimetral turreted wall has a height above ground varying from 1.60 to 4.30 m, with an original estimated value from 4.00 to 5.30 m. The turreted wall has a thickness above the

ground from 2.00 to 4.50 m. The slopes of the facings vary from 2.55° to 7.45°. The entrance stone lintel has an estimated height of approximately 2.40 m. The estimated area of the internal courtyards F, O, and P is 290 m^2. The maximum dimensions of the blocks at the base are 1.90 m width, 0.85 m height, and 1.40 m thickness, and the minimum dimensions are 0.70 m width, 0.40 m height, and 0.80 m thickness. The monument footprint area above the ground is S = 934 m^2. The estimated original footprint is S = 1040 m^2. The maximum dimensions of the above-ground structure are L = 41.10 m × l = 38.74 m × h = 9.70 m. The above-ground volume is V = 2735 m^3.

3.3. Accuracy Assessment

The accuracy of the MVS model can be estimated with the distribution and density of the SfM model tie points, which affects its MVS rebuild quality [17,19]. A uniform distribution of these points on all images contributes to more precise results in dense reconstruction with greater completeness and consistency in 3D reconstruction. The assessment of their density and distribution is an indicator of process quality, especially in the presence of regions with different types of surface textures and in the presence of areas with vegetation and occlusions. In general, the presence of vegetation of various types and densities in the relief area causes occlusion phenomena on the ground that result in a lower accuracy of the 3D model SfM-MVS. To obtain accurate 3D models from SfM-MVS data in vegetation environments, it is critical to consider and eventually remove areas where vegetation may obstruct the view of the underlying terrain. The AI classifier in RC allowed for the division of the entire 3D scene into categories such as "terrain", "monument elements", and "vegetation". In RC, it was possible to segment the areas with vegetation and then interpolate the mesh, reducing the effect of the occluded parts. Integrating nadiral and oblique shots from different angles can partially mitigate the occlusion problem and reduce approximations in 3D reconstruction. The assessment of the accuracy of the model was made on the surfaces of the monument without or with a limited presence of vegetation. Photogrammetric studies estimated errors in the determination of ground control points (GCPs) between 1 and 40 mm, with precisions from 1:300 to <1:1000 for objects with dimensions of $2 \leq D \leq 40$ m. Control measures were acquired using the total station (TS) [13]. Other studies have examined the accuracy of the 3D vertices of mesh derived from Multi-View Stereo (MVS) with precisions up to 1:300–1:1500 for larger areas with buildings in the range of $1 \leq D \leq 10$ m and errors in the range of $0.4 \leq Err \leq 18$ mm. Precisions ranged from 1:2500 to 1:5000 for small objects in the range of $1 \leq D \leq 0.2$ m, and errors were in the range of $0.02 \leq Err \leq 0.7$ mm [13,24,25]. Errors are reported as MEAN, STD, MAE, and RMSE. The use of encoded targets significantly improves the accuracy of the SfM-MVS 3D process by allowing error assessment both globally (reliability of measurements throughout the site) and locally (reliability of reconstructed surfaces from close-up photos) [13]. Using encoded targets, identified with "automatic detection" in RC in the SfM alignment phase, the calculated residue value on GCPs and CPs is lower than those obtained using the set of manually defined constraint points. RTK-GNSS measurements on both natural and coded targets have a similar mean residue variability range. The comparison between the data calculated in the SfM-MVS 3D process and the RTK-GNSS measurements on 9 GCPs and 18 CPs distributed throughout the site shows the residues and statistics in the X (east), Y (north), and Z (height) components. Georeferencing accuracy in SfM on GCPs was calculated with $RMSE_{XY}$ values of 16 mm and $RMSE_{XYZ}$ 19 mm. Instead, the position accuracy on the CPs was calculated in SFM with $RMSE_{XY}$ values of 20 mm and $RMSE_{XYZ}$ 25 mm. The values obtained are comparable with those obtained in other relevant applications and 3D modelling in the archaeological field. The positioning network of GCPs and CPs defined on the monument and in the surrounding area informed the calculation of quality performance and the minimization of the magnitude of errors within the processed point cloud. By analyzing the differences between 3D SfM-MVS coordinate values and RTK-GNSS measurements, the results highlight the quality of the horizontal and vertical precision achieved. The value of the RMSE precision is within ±20 mm for

the RTK-GNSS measurements of the horizontal component and just over ±25 mm for the vertical component (Table 4). Therefore, 3D error is generally affected by higher values of this component. We have observed that the maximum elevation error is found in the highest area of the monument, while the lowest error is in the flat ones.

Table 4. MEAN, STD, MAE, RMSE, $RMSE_{XY}$, and $RMSE_{XYZ}$ error estimation calculated on the GCPs and CPs coordinates during the SfM-MVS process. For each point, the maximal projection error in RC is given in pixels.

GCPs	X (East) (m)	Y (North) (m)	Z (Height) (m)	Error (pix)	CPs	X (East) (m)	Y (North) (m)	Z (Height) (m)	Error (pix)
GCP0	0.000	0.003	0.004	0.227589	CP1	−0.003	0.001	0.004	0.301026
GCP2	−0.001	−0.003	0.000	0.204648	CP3	−0.010	0.035	−0.018	0.275347
GCP5	0.022	0.028	0.017	0.281916	CP4	0.022	0.021	0.022	0.457464
GCP8	−0.027	−0.008	0.018	0.784776	CP6	−0.004	−0.020	−0.023	0.756804
GCP11	−0.002	−0.001	−0.006	0.557855	CP7	−0.021	0.013	0.010	0.312578
GCP12	0.000	0.000	−0.001	0.545884	CP9	−0.011	−0.015	−0.018	0.369149
GCP13	0.002	0.000	0.001	0.347889	CP10	0.000	0.001	0.000	0.341045
GCP15	−0.001	−0.002	−0.002	0.547765	CP14	0.000	0.005	0.001	0.476852
GCP16	−0.002	−0.003	−0.004	0.497452	CP17	0.014	−0.018	0.005	0.388756
MEAN	−0.001	0.002	0.003		CP18	0.024	−0.003	0.023	0.658822
STD	0.012	0.010	0.009		CP19	0.011	0.023	−0.010	0.295589
MAE	0.007	0.006	0.006		CP20	−0.025	−0.008	0.015	0.775562
RMSE	0.012	0.010	0.009		CP21	−0.010	−0.013	−0.011	0.658825
$RMSE_{XY}$	0.016				CP22	0.012	−0.016	0.015	0.612578
$RMSE_{XYZ}$	0.019				CP23	−0.010	−0.013	−0.022	0.425996
					CP24	−0.001	−0.003	−0.003	0.368952
					CP25	0.020	0.002	0.004	0.796852
					CP26	−0.005	−0.004	0.007	0.774135
					MEAN	0.000	−0.001	−0.002	
					STD	0.014	0.015	0.014	
					MAE	0.011	0.012	0.012	
					RMSE	0.014	0.015	0.014	
					$RMSE_{XY}$	0.020			
					$RMSE_{XYZ}$	0.025			

The estimation of the shape errors in terms of the 3D model's rigidity was based on Euclidean distances calculated on the 3D Delaunay triangulation of GCPs (orientation) and CPs (validation) of known coordinates to evaluate the global geometric accuracy of the SfM-MVS 3D model (Figure 14). This method highlights any local deformations that can propagate on the dense point cloud. The calculated RMSE provides a statistical estimation of the error but is sensitive to the presence of systematic errors [17,35]. Low RMSE values indicate that the SfM-MVS 3D model is geometrically accurate and free of significant distortion or systematic errors (Table 5). In particular, the value of the RMSE for the Euclidean distances calculated on CPs was <20 mm with a maximum accuracy value of 1/4000. This value can be considered acceptable for this study compared to the extent of the surveyed area and the size of the monument.

The surface deviation errors estimation is based on a validation method of 3D SfM-MVS models without using the laser scanner as "ground truth". A photogrammetric benchmark was set as a reference model with the same APS-C sensor used for the survey. On the typical surface (consisting of the face of a tower of the perimetral wall), the photogrammetric clouds obtained using this APS-C sensor achieve results comparable to those of a full-frame DSLR camera with an absolute cloud-to-cloud distance (C2C) error of <1.44 cm at the 95th percentile (Q_{95}) after removing outlier values with errors higher than the 99th percentile (Q_{99}). These values are within the limits required for mapping architectural heritage. C2C comparison operating on the XY and XZ planes has the advantage of highlighting any rough errors present in the 3D data. Major errors on individual XY and XZ planes emerge immediately, affecting the overall statistical distribution of distances with larger values. Thus, with such a comparison, we could effectively detect both systematic differences in accuracy and significant localized errors in the 3D point clouds where there are occlusion areas with effects on the completeness of reconstructed surfaces.

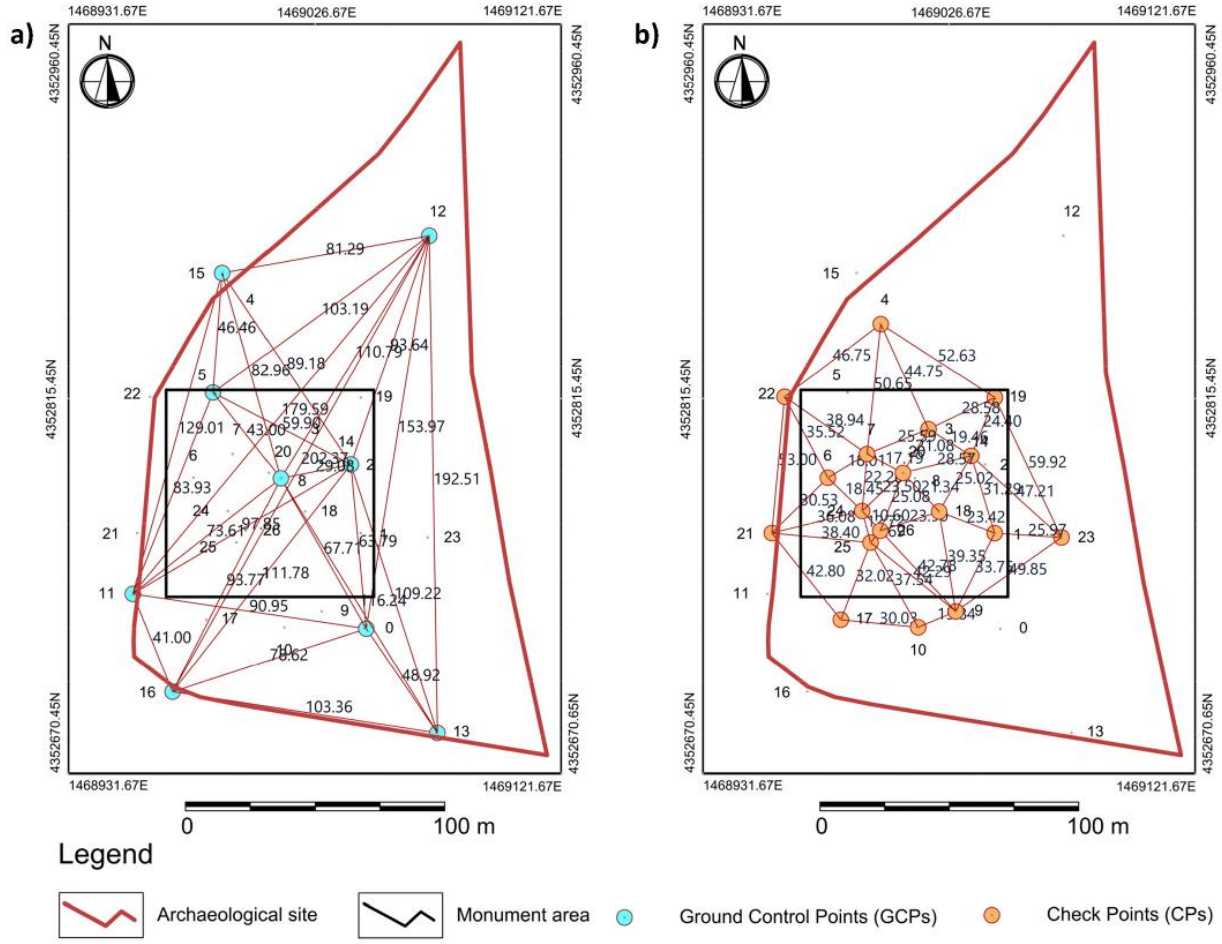

Figure 14. (**a**) View of the 3D Delaunay triangulation of GCPs (orientation) and (**b**) CPs (validation) to perform the error estimation of the SfM-MVS 3D model based on Euclidean distances.

Table 5. Estimation of RMSE errors based on Euclidean distances computed with SfM-MVS process and measured values (MD = measured distance, ΔD = absolute error difference).

GCPs (MD) (m)	ΔD (m)	CPs (MD) (m)	ΔD (m)	CPs (MD) (m)	ΔD (m)	CPs (MD) (m)	ΔD (m)
29.08	0.010	6.69	0.005	32.15	0.022	52.63	0.021
41.00	0.012	10.60	0.010	33.75	0.018	53.00	0.013
43.00	0.014	12.72	0.010	35.52	0.022	55.36	0.022
46.46	0.017	15.84	0.014	35.62	0.023	56.02	0.019
48.92	0.019	17.19	0.010	36.08	0.018	57.03	0.017
59.90	0.018	18.01	0.017	37.54	0.019	57.19	0.023
63.79	0.016	18.45	0.015	37.99	0.018	58.20	0.021
67.71	0.017	19.46	0.010	38.40	0.017	58.77	0.022
73.61	0.019	21.08	0.020	38.94	0.018	59.92	0.019
78.62	0.021	21.34	0.020	39.35	0.020	61.07	0.024
81.29	0.015	22.20	0.015	40.31	0.021	62.87	0.026
82.96	0.016	23.42	0.018	40.71	0.020	65.31	0.024
83.93	0.019	23.50	0.015	42.28	0.018	67.35	0.029
89.18	0.018	23.90	0.015	42.29	0.016	71.54	0.027
90.95	0.021	24.40	0.021	42.78	0.014	73.75	0.028
93.64	0.019	25.02	0.020	42.80	0.018	73.81	0.028

Table 5. *Cont.*

GCPs (MD) (m)	ΔD (m)	CPs (MD) (m)	ΔD (m)	CPs (MD) (m)	ΔD (m)	CPs (MD) (m)	ΔD (m)
93.77	0.022	25.08	0.010	43.22	0.019	81.21	0.030
97.85	0.020	25.59	0.017	43.65	0.017	90.93	0.032
103.19	0.019	25.97	0.015	44.75	0.017	100.81	0.030
103.36	0.021	28.57	0.016	46.75	0.021	111.83	0.035
109.22	0.024	28.58	0.018	46.87	0.019	-	-
110.79	0.023	29.35	0.022	47.21	0.018	-	-
111.78	0.023	29.89	0.018	47.22	0.019	-	-
116.24	0.024	30.02	0.019	47.24	0.017	-	-
129.01	0.023	30.03	0.022	48.03	0.020	-	-
153.97	0.022	30.53	0.015	49.85	0.018	-	-
179.59	0.017	30.86	0.018	50.65	0.024	-	-
192.51	0.022	31.29	0.017	51.38	0.027	-	-
202.37	0.025	32.02	0.019	52.42	0.019	-	-
RMSE	0.019					RMSE	0.020

Benchmarks on the typical surfaces were used for both SfM-MVS validation and the geometric simplification of the 3D model. Through the C2C comparison of the typical surfaces representing the geometric variability of the wall faces, the surface deviation error of the SfM-MVS model was estimated and the simplified process was guided with the combined use of RC and CC software (Figure 15). On the surface of tower M with a simplified edge length of 2 cm, the C2C error was <2.30 cm at Q_{95} after removing outlier values with errors higher than the Q_{99} percentile. With a simplified edge length of 3 cm, the C2C error was <2.9 cm at Q_{95} after removing outlier values with errors higher than Q_{99} (Tables 6 and 7). This integrated methodology allowed for the identification of the optimal level of simplification of the model (minimum length of the edges), keeping the error within the limits set by the study according to the specifications of the survey and the digital representation of the monument. In addition, the texture reprojection in RC from the original models to the simplified models allowed the high visual quality of the 3D reconstruction to be maintained.

Table 6. "Ground Truth" data acquisition setting and cloud-to-cloud (C2C) deviation analysis on M tower. Mean (M), standard deviation (STD), root mean square (RMS), and absolute errors on fitted Gaussian distribution at 95th percentile (Q_{95}).

Photos n	H (m)	GSD (cm/pix)	RR_4 (m)	Dw (m)	Dh (m)	B/H	Cloud-to-Cloud (C2C) (Fitted Gaussian Distribution)	M (m)	STD (m)	RMS (m)	Q_{95} (m)
35	5	0.13	$8 \times 5 \times 2$ m	6.48	4.29	0.2	XYZ	0.007	0.004	0.009	0.014

Table 7. Progressively simplified minimal edge length. "Ground Truth" and survey cloud-to-cloud (C2C) deviation analysis estimation. Mean (M), standard deviation (STD), root mean square (RMS), and absolute errors on fitted Gaussian distribution at 95th percentile (Q_{95}).

Simplify Minimal Edge Length (cm)	Cloud-to-Cloud (C2C) (Fitted Gaussian Distribution)	M (m)	STD (m)	RMS (m)	Q_{95} (m)
1	XYZ	0.007	0.004	0.009	0.014
2	XYZ	0.013	0.006	0.014	0.023
3	XYZ	0.018	0.007	0.019	0.029

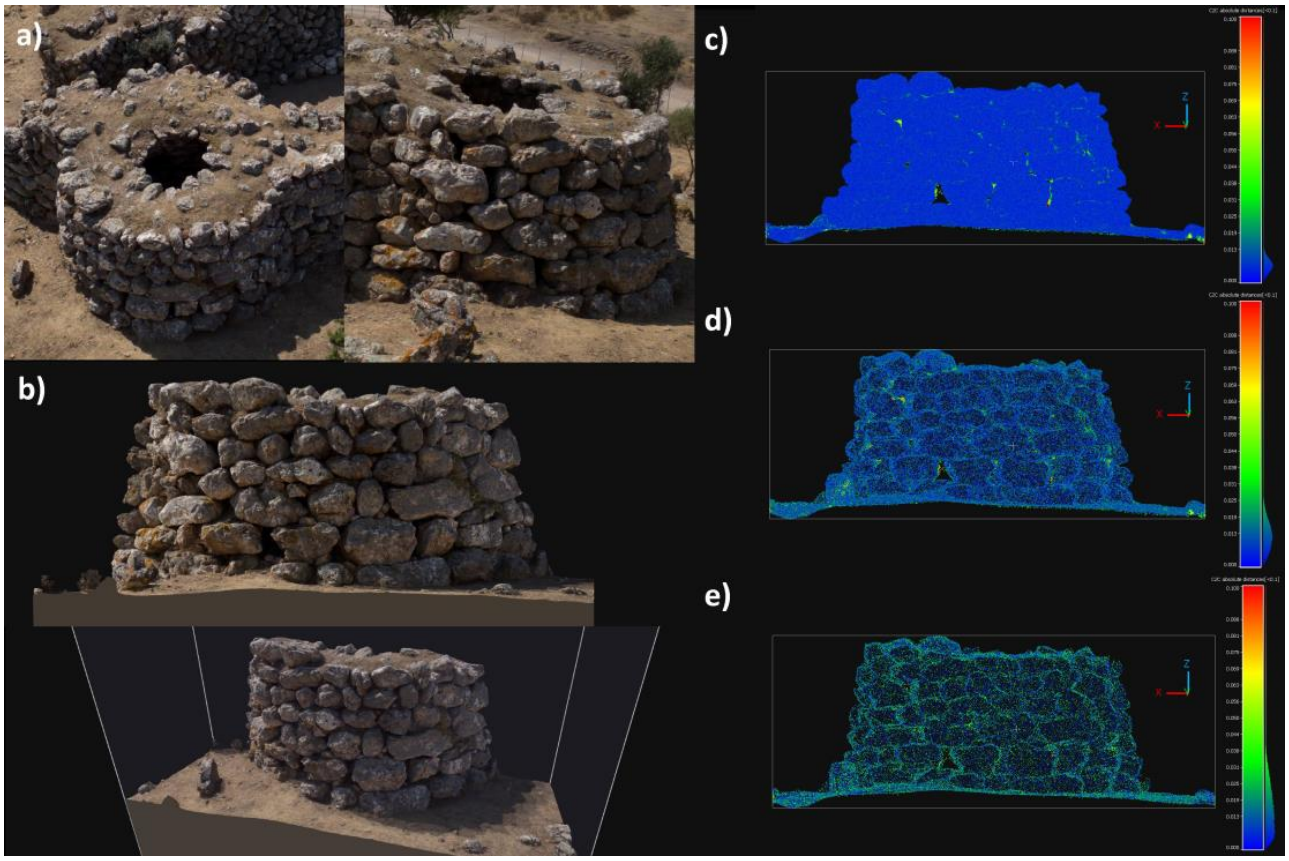

Figure 15. (**a**) Top view from north of detail tower M; (**b**) example of model surface for C2C comparison: the wall of tower M, with the 3D model delimited by the reconstruction region (RR_4); (**c**) the calculated distance from C2C of point clouds M1 and M2; (**d**,**e**) the calculated C2C error distance from point clouds with progressive simplification of the minimal edge length.

4. Discussion

Georeferencing was a key moment in the 3D reconstruction and topographic mapping of the surveyed area. The errors in the photogrammetric survey for GCPs and CPs are less than or equal to those of RTK-GNSS point acquisition. The workflow employed here allowed for the systematic definition of flight parameters, the photogrammetric acquisition of aerial and terrestrial schemes for the APS-C sensor used, the definition of the best distribution of GCPs, and the processing of photogrammetric data for the 3D modelling of the monument [13,18,27,28,31,33]. From the results obtained by comparing the compositional characteristics of the building materials with the geomaterials sampled during the geoarchaeological survey, it is evident that blocks from the slopes of Mount Acqua and the deposits of the Rio San Giovanni riverbed, worked by the action of the river current, were used for the construction of the Nuraghe. Many of these blocks, in fact, show a very close similarity in shape and size with those used in the Nuraghe. The definition of the typological characterization of the materials and the attribution of provenance areas are decisive in enriching the knowledge of the technological level reached by the Nuragic civilization. It is evident that although the stone materials used are not suited for the best shape regularization, due to their extreme hardness, the monument was built with an extremely advanced knowledge of building statics. The well-established construction technique of Nuraghes was masterfully adapted here to take advantage of the natural shapes of the boulders, without necessarily having to reshape them, enabling the construction of this impressive structure. Despite the widespread collapses and discontinuities, thanks to the processing of 2D and 3D digital models, the architecture of the monument is now well defined, allowing us to provide useful information to support future historical and

archaeological studies regarding the actual proportions and dimensions that the monument must have had in its period of full functionality. The elaboration of the TIN of the basement allowed us to estimate the elevation of the rocky outcrops at the foundation of the Nuraghe and to define the lower levels of the entrances, which are currently also not visible due to the covering of materials from the numerous collapses of the structures. This also allowed us to estimate, with reasonable certainty, the thicknesses of collapse material that would have to be removed to obtain to the original floor level in the interior chambers. This also allowed us to obtain numerical data to propose a hypothesis about the actual original dimensions of the monument.

5. Conclusions

The proposed work represents part of a larger project on 3D reconstruction and virtualization in historical and archaeological settings, from the scale of the find to the scale of the site. This is to gain a better understanding of the state of preservation through dimensional analysis based on digital models and to hypothesize the original dimensions and shapes through the analysis of the archaeological remains. The approach used to perform the photogrammetric survey of the archaeological area in question and the workflow adopted in the photogrammetric process resulted in accurate 3D models according to the study specifications. In this study, we evaluated the accuracy and quality of the SfM-MVS 3D reconstruction of a Nuraghe using images acquired through aerial (UAV) and terrestrial surveys with an APS-C sensor. The validation process of the SfM-MVS model, through the estimation of position, rigidity, and surface deviation errors, allowed us to assess the accuracy and precision in terms of the robustness and completeness of the 3D model. Based on the study's objectives, the global geometric consistency of the reconstructed model and the visual quality of its surfaces were verified. We also demonstrated how the treatment and simplification of point clouds enabled the optimization of the obtained digital models. The results of this study show that for structures like those surveyed and under specific survey conditions, the use of high-quality APS-C sensors provides operational flexibility, allowing the acquisition configuration to be adapted to the specific needs of the survey. The versatility of APS-C sensors, which can be mounted on UAVs, telescopic masts, tripods, and three-axis stabilizers, enables efficient image capture under optimal operating conditions. This adaptability ensures the comprehensive coverage of the surveyed site in terms of the acquisition of images, improving the quality of the 3D reconstruction. The analysis of building materials and the geolithological context led to the identification of the areas of supply of local geomaterials used for the construction of the Nuragic monument. Of these, in particular, the blocks were skillfully selected for shape and size so that they could be used as is, without any reshaping. The results of our research provide the basic and indispensable documentation for the planning of maintenance and securing of the archaeological site, for the planning of future excavation campaigns, and for the planning of conservation restoration work. As of now, the 3D digital drawings have also been earmarked for purposes of enhancing the archaeological site through digital media and for promotion for tourism purposes. Future developments in our research will be oriented toward testing different data processing strategies with SfM-MVS integrated with LiDAR and laser scanner technologies. Different types of monuments and artefacts at different scales will be studied employing systems using new volumetric rendering techniques and advanced 3D visualization. The collection, management, and analysis of the photographic datasets according to the proposed workflow, in addition to representing a digital asset for each monument studied, will be able to improve, in a multidisciplinary context, the potential for the investigation and analysis of archaeological artefacts and Nuragic sites for the enhancement of cultural heritage.

Author Contributions: Conceptualization of photogrammetric methodology integrated with contribution to material analysis, S.C., C.M. and P.V.; photogrammetric survey planning and data acquisition, S.C. and C.M.; processing methodology, interpretation, and visualization of photogrammetric data, C.M.; XRD analysis, geoarchaeological survey, and sampling, S.C. All authors analyzed and discussed the results of the work and contributed to the drafting and revision of the manuscript. All authors have read and agreed to the published version of the manuscript.

Funding: The APC was funded by the Fondazione di Sardegna, grant number F73C22001270007 (P. Valera).

Data Availability Statement: Data are contained within the article.

Acknowledgments: We are very grateful to the Archaeological Superintendents of Cagliari and Oristano and to the Consorzio Natura Viva Sardegna of Domusnovas for providing access to the archaeological area. We also wish to thank Michal Jancosek for supporting our research with the advanced photogrammetry software RealityCapture.

Conflicts of Interest: The authors declare no conflicts of interest.

References

1. Lilliu, G. *I Nuraghi. Torri Preistoriche Della Sardegna*; Cambridge University Press: Cambridge, UK, 1962.
2. Lilliu, G. *La Civiltà dei Sardi dal Paleolitico alla Fine dell'età Nuragica*; Maestrale: Torino, Italy, 1988.
3. Contu, E. *L'architettura Nuragica*; 1981 in AA.VV; Libri Scheiwiller: Milano, Italy, 1981; pp. 1–178.
4. Contu, E. *La Sardegna Preistorica e Nuragica*; Carlo Delfino Editore: Sassari, Italy, 1998; Volume I–II.
5. Melis, P. I Nuraghi. In *la Sardegna Nuragica. Storia e Monumenti, Regione Autonoma della Sardegna/Carlo Delfino Editore*; Moravetti, A., Melis, P., Foddai, L., Alba, E., Eds.; Carlo Delfino Editore: Sassari, Italy, 2017; pp. 29–53, ISBN 978-88-7138-995-0.
6. Ugas, G. La Sardegna Nuragica. Aspetti Generali. In *LA SARDEGNA NURAGICA, Storia e Materiali*; Moravetti, A., Alba, E., Foddai, L., Eds.; Carlo Delfino Editore: Sassari, Italy, 2014; pp. 11–34, ISBN 978-88-7138-750-5.
7. Cossu, T.; Perra, M.; Usai, A. *Il Tempo dei Nuraghi. La Sardegna dal XVIII al VIII Secolo a.C.*; Ilisso: Cagliari, Italy, 2018; ISBN 978-88-6202-366-5.
8. Usai, A. *The Nuragic Adventure: Monuments, Settlements and Landscapes*; McDonald Institute for Archaeological Research: Cambridge, UK, 2021; pp. 155–169. [CrossRef]
9. Perra, M. I modelli di nuraghe come memoria collettiva di una civiltà. In *LA SARDEGNA NURAGICA, Storia e Monumenti*; Moravetti, A., Melis, P., Alba, E., Foddai, L., Eds.; Carlo Delfino Editore: Sassari, Italy, 2017; pp. 67–84, ISBN 978-88-7138-995-0.
10. Della Marmora, A. *Voyage En Sardaigne, Ou, Description Statistique, Physique Et Politique De Cette Île: Avec Des Recherches Sur Ses Productions Naturelles Et Ses Antiquités*; Biodiversity Heritage Library: Washington, DC, USA, 2022; Volume 1, ISBN 978-1017400939.
11. Della Marmora, A. *Itinerario dell'Isola di Sardegna (Titolo Originale "Itinéraire de l'Ile de Sardaigne, Pour Faire Suite au Voyage en Cette Contrée, Tome I–II)*; Ilisso: Cagliari, Italy, 1860; ISBN 9788862021081.
12. Vanzetti, A.; Castangia, G.D.; Depalmas, A.; Ialongo, N.; Leonelli, V.; Perra, M.; Usai, A. Complessi fortificati della Sardegna e delle isole del mediterraneo occidentale nella protostoria. In *Scienze Dell'antichità, Sapienza Università di Roma, Dipartimento di Scienze Dell'antichità*; Edizioni Quasar: Roma, Italy, 2013; Volume 19, pp. 2–3.
13. Sapirstein, P. Accurate measurement with photogrammetry at large sites. *J. Archaeol. Sci.* **2016**, *66*, 137–145. [CrossRef]
14. Kingsland, K. Comparative analysis of digital photogrammetry software for cultural heritage. *Digit. Appl. Archaeol. Cult. Heritage* **2020**, *18*, e00157. [CrossRef]
15. Massimiliano, P.; Domenica, C. UAV Photogrammetry and 3D Modelling of Complex Architecture for Maintenance Purposes: The Case Study of the Masonry Bridge on the Sele River, Italy. *Period. Polytech. Civ. Eng.* **2021**, 191–203. [CrossRef]
16. Marín-Buzón, C.; Pérez-Romero, A.; López-Castro, J.L.; Jerbania, I.B.; Manzano-Agugliaro, F. Photogrammetry as a New Scientific Tool in Archaeology: Worldwide Research Trends. *Sustainability* **2021**, *13*, 5319. [CrossRef]
17. Janiszewski, M.; Torkan, M.; Uotinen, L.; Rinne, M. Rapid Photogrammetry with a 360-Degree Camera for Tunnel Mapping. *Remote. Sens.* **2022**, *14*, 5494. [CrossRef]
18. Pepe, M.; Alfio, V.S.; Costantino, D. UAV Platforms and the SfM-MVS Approach in the 3D Surveys and Modelling: A Review in the Cultural Heritage Field. *Appl. Sci.* **2022**, *12*, 12886. [CrossRef]
19. Vlachos, M.; Berger, L.; Mathelier, R.; Agrafiotis, P.; Skarlatos, D. Software comparison for underwater archaeological photogrammetric applications. *Int. Arch. Photogramm. Remote Sens. Spat. Inf. Sci.* **2019**, *XLII-2/W15*, 1195–1201. [CrossRef]
20. Lingua, A.; Noardo, F.; Spanò, A.; Sanna, S.; Matrone, F. 3D model generation using oblique images acquired by UAV. *Int. Arch. Photogramm. Remote Sens. Spat. Inf. Sci.* **2017**, *XLII-4/W2*, 107–115. [CrossRef]
21. Cara, S.; Fiori, M.; Matzuzzi, C. Assessment of landscape by photogrammetry proximity UAV survey technique: A case study of an abandoned mine site in the Furtei area (Sardinia-Italy). In Proceedings of the 23rd International Mining Congress and Exhibition of Turkey, IMCET, Antalya, Turkey, 16–19 April 2013; Volume 1, pp. 83–92.

22. Cara, S.; Fiori, M.; Matzuzzi, C. Unmanned aerial vehicle system-based remote sensing for monitoring landscape degradation. In Proceedings of the International Multidisciplinary Scientific GeoConference Surveying Geology and Mining Ecology Management, SGEM 2017, Vienna, Austria, 27–29 November 2017; Volume 17, pp. 309–316.
23. James, M.R.; Robson, S. Mitigating systematic error in topographic models derived from UAV and ground-based image networks. *Earth Surf. Process. Landf.* **2014**, *39*, 1413–1420. [CrossRef]
24. Cara, S.; Valera, P.; Matzuzzi, C. Morphometric Analysis through 3D Modelling of Bronze Age Stone Moulds from Central Sardinia. *Minerals* **2021**, *11*, 1192. [CrossRef]
25. Casula, G.; Fais, S.; Cuccuru, F.; Bianchi, M.G.; Ligas, P. Diagnostic Process of an Ancient Colonnade Using 3D High-Resolution Models with Non-Invasive Multi Techniques. *Sensors* **2023**, *23*, 3098. [CrossRef] [PubMed]
26. Tahar, K.N. Height accuracy based on different RTK GPS method for ultra-light aircraft images. In Proceedings of theThe International Archives of the Photogrammetry, Remote Sensing and Spatial Information Sciences, Volume XL-3/W3, 2015 ISPRS Geospatial Week, La Grande Motte, France, 28 September–3 October 2015; pp. 287–292. [CrossRef]
27. Mora, O.E.; Suleiman, A.; Chen, J.; Pluta, D.; Okubo, M.H.; Josenhans, R. Comparing sUAS Photogrammetrically-Derived Point Clouds with GNSS Measurements and Terrestrial Laser Scanning for Topographic Mapping. *Drones* **2019**, *3*, 64. [CrossRef]
28. Barba, S.; Barbarella, M.; Di Benedetto, A.; Fiani, M.; Gujski, L.; Limongiello, L. Accuracy Assessment of 3D Photogrammetric Models from an Unmanned Aerial Vehicle. *Drones* **2019**, *3*, 79. [CrossRef]
29. Lai, L.; Sordini, M.; Campana, S.; Usai, L.; Condò, F. 4D recording and analysis: The case study of Nuraghe Oes (Giave, Sardinia). *Digit. Appl. Archaeol. Cult. Herit.* **2015**, *2*, 233–239. [CrossRef]
30. Moyano, J.; Nieto-Julián, J.E.; Bienvenido-Huertas, D.; Marín-García, D. Validation of Close-Range Photogrammetry for Architectural and Archaeological Heritage: Analysis of Point Density and 3D Mesh Geometry. *Remote Sens.* **2020**, *12*, 3571. [CrossRef]
31. RealityCapture Software, Version 1.3.1.117316 [CLI Software]. Epic Game Slovakia s.r.o., Slovakia. Available online: https://www.capturingreality.com (accessed on 20 March 2024).
32. Ezequiel, F.G.; Aguera-Vega, F.; Carvajal-Ramirez, F.; Martinez-Carricondo, P. UAV Photogrammetry Accuracy Assessment for Corridor Mapping Based on the Number and Distribution of Ground Control Points. *Remote Sens.* **2020**, *12*, 2447. [CrossRef]
33. Cucci, D.A. Accurate optical target pose determination for applications in aerial photogrammetry. In Proceedings of the SPRS Annals of the Photogrammetry, Remote Sensing and Spatial Information Sciences, XXIII ISPRS Congress, Prague, Czech Republic, 12–19 July 2016; Volume III-3; pp. 257–262. [CrossRef]
34. Guo, X.; Chen, Y.; Wang, C.; Cheng, M.; Wen, C.; Yu, J. Automatic shape-based target extraction for close-range photogrammetry. In Proceedings of the International Archives of the Photogrammetry, Remote Sensing and Spatial Information Sciences, Volume XLI-B1, 2016 XXIII ISPRS Congress, Prague, Czech Republic, 12–19 July 2016; pp. 583–587. [CrossRef]
35. Nocerino, E.; Stathopoulou, E.K.; Rigon, S.; Remondino, F. Surface Reconstruction Assessment in Photogrammetric Applications. *Sensors* **2020**, *20*, 5863. [CrossRef] [PubMed]
36. MikroKopter, 2024 HiSystems GmbH. Website for MikroKopter Do-It-Yourself Construction. Available online: https://doc.mikrokopter.de/ (accessed on 20 March 2024).
37. Wojciech, A.D. Exploiting the Redundancy of Multiple Overlapping Aerial Images for Dense Image Matching Based Digital Surface Model Generation. *Remote Sens.* **2017**, *9*, 490. [CrossRef]
38. Jancosek, M.; Shekhovtsov, A.; Pajdla, T. Scalable Multi-View Stereo. In Proceedings of the IEEE 12th International Conference on Computer Vision, ICCV Workshops, Kyoto, Japan, 27 September–4 October 2009; pp. 1526–1533. [CrossRef]
39. Jancosek, M.; Pajdla, T. Multi-view reconstruction preserving weakly-supported surface. In Proceedings of the IEEE Conference on Computer Vision and Pattern Recognition, Colorado Springs, CO, USA, 20–25 June 2011. [CrossRef]
40. Cloud Compare, Version 2.12.4 [GNU GPL Software]. 2021. Available online: http://www.cloudcompare.org (accessed on 20 March 2024).
41. Note Illustrative della Carta Geologica d'Italia 1:50.000, Foglio 555 Iglesias, 2015, ISPRA, Servizio Geologico d'Italia, Regione Autonoma della Sardegna. Available online: https://hdl.handle.net/20.500.11769/103033 (accessed on 20 March 2024).